

Analysis of the dynamics of the decay

$$D^+ \rightarrow K_S^0 \pi^0 e^+ \nu_e$$

The BESIII collaboration



ABSTRACT: The branching fraction of $D^+ \rightarrow K_S^0 \pi^0 e^+ \nu_e$ is measured for the first time using 7.93 fb^{-1} of e^+e^- annihilation data collected at the center-of-mass energy $\sqrt{s} = 3.773 \text{ GeV}$ with the BESIII detector operating at the BEPCII collider, and is determined to be $\mathcal{B}(D^+ \rightarrow K_S^0 \pi^0 e^+ \nu_e) = (0.881 \pm 0.017_{\text{stat.}} \pm 0.016_{\text{syst.}})\%$. Based on an analysis of the $D^+ \rightarrow K_S^0 \pi^0 e^+ \nu_e$ decay dynamics, we observe the S -wave and P -wave components with fractions of $f_{S\text{-wave}} = (6.13 \pm 0.27_{\text{stat.}} \pm 0.30_{\text{syst.}})\%$ and $f_{\bar{K}^*(892)^0} = (93.88 \pm 0.27_{\text{stat.}} \pm 0.29_{\text{syst.}})\%$, respectively. From these results, we obtain the branching fractions $\mathcal{B}(D^+ \rightarrow (K_S^0 \pi^0)_{S\text{-wave}} e^+ \nu_e) = (5.41 \pm 0.35_{\text{stat.}} \pm 0.37_{\text{syst.}}) \times 10^{-4}$ and $\mathcal{B}(D^+ \rightarrow \bar{K}^*(892)^0 e^+ \nu_e) = (4.97 \pm 0.11_{\text{stat.}} \pm 0.12_{\text{syst.}})\%$. In addition, the hadronic form-factor ratios of $D^+ \rightarrow \bar{K}^*(892)^0 e^+ \nu_e$ at $q^2 = 0$, assuming a single-pole dominance parameterization, are determined to be $r_V = \frac{V(0)}{A_1(0)} = 1.43 \pm 0.07_{\text{stat.}} \pm 0.03_{\text{syst.}}$ and $r_2 = \frac{A_2(0)}{A_1(0)} = 0.72 \pm 0.06_{\text{stat.}} \pm 0.02_{\text{syst.}}$.

KEYWORDS: Charm vector, Branching fraction measurement, Helicity amplitude analysis

Contents

1	INTRODUCTION	1
2	BESIII DETECTOR AND MONTE CARLO SIMULATION	2
3	METHOD	3
4	SINGLE-TAG SELECTION	3
5	DOUBLE-TAG SELECTION	4
6	BRANCHING FRACTION	6
7	SYSTEMATIC UNCERTAINTY OF BRANCHING FRACTION	7
8	AMPLITUDE ANALYSIS OF $D^+ \rightarrow K_S^0 \pi^0 e^+ \nu_e$	8
8.1	<i>S</i> -WAVE FORM FACTOR	10
8.2	<i>P</i> -WAVE FORM FACTOR	11
8.3	AMPLITUDE-ANALYSIS METHOD	12
8.4	SYSTEMATIC UNCERTAINTY OF AMPLITUDE ANALYSIS	14
9	SUMMARY	16

1 INTRODUCTION

Semileptonic D decays play an important role in our understanding of strong and weak effects in the charm sector [1–3]. Measurements of these semileptonic decay rates offer an opportunity to determine the Cabibbo-Kobayashi-Maskawa (CKM) matrix elements, which describe the quark-flavor mixing of the weak interaction in the standard model (SM) [4–6]. The strong interaction is characterized by the hadronic form factors that define the initial and final hadrons. Various theoretical models, such as Lattice QCD [7–12], the quark model [13–15], and QCD sum rules [16], make predictions for the branching fractions (BFs) or hadronic form factors of $D \rightarrow K^*$ transitions. The measurements of the BFs or hadronic form factors of $D^+ \rightarrow \bar{K}^{*0} e^+ \nu_e$ are therefore valuable for testing and validating these theoretical calculations [7–16].

Experimental measurements of the BFs and form factors of $D^+ \rightarrow \bar{K}^{*0} e^+ \nu_e$ via $\bar{K}^{*0} \rightarrow K^- \pi^+$ have been reported by various experiments, including MARKIII [17], CLEO-c [18], BaBar [19], and BESIII [20], and are summarized by the Particle Data Group (PDG) [21]. However, no experimental study of $D^+ \rightarrow \bar{K}^{*0} e^+ \nu_e$ via $\bar{K}^{*0} \rightarrow \bar{K}^0 \pi^0$ has yet been performed. The $D^+ \rightarrow K_S^0 \pi^0 e^+ \nu_e$ decay is expected to be dominated by $D^+ \rightarrow \bar{K}^{*0} e^+ \nu_e$,

which is mediated via the Feynman diagram shown in Fig. 1. In this paper, we present the first study of the $D^+ \rightarrow K_S^0 \pi^0 e^+ \nu_e$ decay dynamics. This analysis is based on a data sample of e^+e^- collisions collected at a center-of-mass energy of $\sqrt{s} = 3.773$ GeV by the BESIII detector operating at the BEPCII collider in 2010, 2011, and 2021, and correspond to a total integrated luminosity of 7.93 fb^{-1} [22]. Throughout this paper, the charge conjugate channels are always implied.

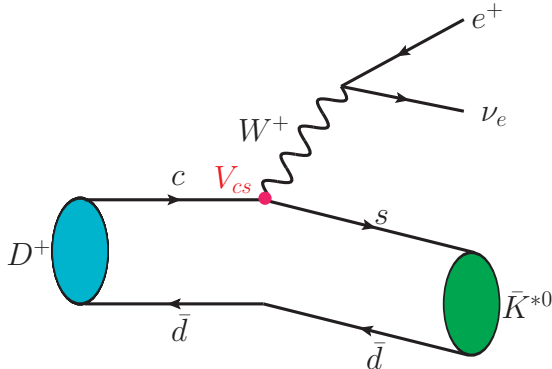


Figure 1. The Feynman diagram of the $D^+ \rightarrow \bar{K}^{*0} e^+ \nu_e$ decay.

2 BESIII DETECTOR AND MONTE CARLO SIMULATION

The BESIII detector [23] records symmetric e^+e^- collisions provided by the BEPCII storage ring [24] in the center-of-mass energy range from 2.00 to 4.95 GeV, with a peak luminosity of $1.1 \times 10^{33} \text{ cm}^{-2}\text{s}^{-1}$ achieved at $\sqrt{s} = 3.77$ GeV. BESIII has collected large data samples in this energy region [25–27]. The cylindrical core of the BESIII detector [28] covers 93% of the full solid angle and consists of a helium-based multilayer drift chamber (MDC), a plastic scintillator time-of-flight system (TOF), and a CsI(Tl) electromagnetic calorimeter (EMC), which are all enclosed in a superconducting solenoidal magnet providing a 1.0 T magnetic field.

The solenoid is supported by an octagonal flux-return yoke with resistive plate counter muon identification modules interleaved with steel. The charged-particle momentum resolution at 1 GeV/c is 0.5%, and the dE/dx resolution is 6% for electrons from Bhabha scattering. The EMC measures photon energies with a resolution of 2.5% (5%) at 1 GeV in the barrel (end-cap) region. The time resolution in the TOF barrel region is 68 ps, while that in the end-cap region of data collected before 2015 is 110 ps. The end-cap TOF system was upgraded in 2015 using multigap resistive plate chamber technology, providing a time resolution of 60 ps, which benefits 83% of the data used in this analysis [29].

Simulated event samples produced with the GEANT4-based [30] Monte Carlo (MC) package, which includes the geometric description of the BESIII detector and the detector response, are used to determine the detection efficiency and estimate backgrounds. The simulation includes the beam-energy spread and initial-state radiation in the e^+e^- annihilations modeled with the KKMC generator [31]. An inclusive MC sample includes the

production of $D\bar{D}$ pairs (including quantum coherence for the neutral D channels), the non- $D\bar{D}$ decays of the $\psi(3770)$, the initial-state radiation production of the J/ψ and $\psi(3686)$ states, and the continuum processes incorporated in KKMC [31]. All particle decays are modelled with EVTGEN [32] using the BFs either taken from the Particle Data Group [21], when available, or otherwise estimated with LUNDCHARM [33]. Final-state radiation from charged particles is incorporated with the PHOTOS package [34].

In this paper, the inclusive MC sample is used to determine the selection efficiencies of the tag side and to estimate the backgrounds. The signal MC samples of $D^+ \rightarrow K_S^0 \pi^0 e^+ \nu_e$, which are used to determine the signal efficiency, are simulated with the parameters obtained from the amplitude-analysis fit.

3 METHOD

At $\sqrt{s} = 3.773$ GeV, D^+D^- meson pairs are produced from $\psi(3770)$ decays without accompanying hadrons, providing an ideal opportunity to study semileptonic D^+ decays using the double-tag (DT) method [35]. Initially, single-tag (ST) D^- mesons are reconstructed via the decays $D^- \rightarrow K^+ \pi^- \pi^-$, $K_S^0 \pi^-$, $K^+ \pi^- \pi^- \pi^0$, $K_S^0 \pi^- \pi^0$, $K_S^0 \pi^+ \pi^- \pi^-$, and $K^+ K^- \pi^-$. Subsequently, the semileptonic D^+ candidates are reconstructed by using the remaining tracks that were not utilized in the ST selection. An event in which the semileptonic decay $D^+ \rightarrow K_S^0 \pi^0 e^+ \nu_e$ is reconstructed in the system recoiling against the ST D^- mesons is referred to as a DT event. The BF of $D^+ \rightarrow K_S^0 \pi^0 e^+ \nu_e$ is determined by

$$\mathcal{B}_{\text{SL}} = \frac{N_{\text{DT}}}{N_{\text{ST}}^{\text{tot}} \bar{\epsilon}_{\text{sig}} \mathcal{B}_{K_S^0} \mathcal{B}_{\pi^0}}, \quad (3.1)$$

where $N_{\text{ST}}^{\text{tot}}$ and N_{DT} represent the yields of the ST D^- mesons and the DT signal events in data, respectively; $\mathcal{B}_{K_S^0}$ and \mathcal{B}_{π^0} are the BFs of $K_S^0 \rightarrow \pi^+ \pi^-$ and $\pi^0 \rightarrow \gamma\gamma$, respectively, as reported by the PDG [21]. $\bar{\epsilon}_{\text{sig}}$ denotes the average signal efficiency weighted by the measured yield of tag mode i in the data, i.e.,

$$\bar{\epsilon}_{\text{sig}} = \frac{\sum_i (N_{\text{ST}}^i \cdot \epsilon_{\text{DT}}^i / \epsilon_{\text{ST}}^i)}{N_{\text{ST}}^{\text{tot}}}, \quad (3.2)$$

where N_{ST}^i is the yield of the observed ST candidates in data, ϵ_{ST}^i is the efficiency of reconstructing the ST mode i (called the ST efficiency), and ϵ_{DT}^i is the efficiency of finding the ST mode i and the $D^+ \rightarrow K_S^0 \pi^0 e^+ \nu_e$ decay simultaneously (called the DT efficiency).

4 SINGLE-TAG SELECTION

For each charged track (except those used for K_S^0 reconstruction), the polar angle with respect to the MDC axis (θ) must satisfy $|\cos \theta| < 0.93$, and the point of closest approach to the interaction point (IP) must lie within 1 cm in the plane perpendicular to the MDC axis and within 10 cm along the MDC axis. Charged tracks are identified using the dE/dx and TOF information, from which the combined confidence levels under the pion and kaon

hypotheses are separately computed. The charged tracks are then assigned to the particle type with the higher probability.

Candidates for K_S^0 are formed from pairs of oppositely charged tracks. For these two tracks, the distance of closest approach to the IP is required to be less than 20 cm along the MDC axis. There are no limitations on the distance of closest approach in the transverse plane or particle-identification (PID) criteria for these tracks. The two charged tracks are constrained to originate from a common vertex, which must be at least twice the vertex resolution away from the IP in terms of flight distance. The quality of the vertex fits (primary vertex fit and second vertex fit) is ensured by a requirement on the χ^2 ($\chi^2 < 100$). The invariant mass of the $\pi^+\pi^-$ pair is required to be within $(0.487, 0.511)$ GeV/ c^2 .

Neutral-pion candidates are reconstructed via the $\pi^0 \rightarrow \gamma\gamma$ decay. The EMC time deviation from the event start time is required to lie within $[0, 700]$ ns. The energy deposited in the EMC is required to be greater than 25 MeV in the barrel region ($|\cos\theta| < 0.80$) and 50 MeV in the end cap ($0.86 < |\cos\theta| < 0.92$). The opening angle between the photon candidate and the nearest charged track in the EMC is required to be greater than 10° . At least one of the photons is required to be detected in the barrel EMC as the end caps have significantly worse resolution than the barrel. For each π^0 candidate, the invariant mass of the photon pair is required to be within $(0.115, 0.150)$ GeV/ c^2 . To improve the momentum resolution, a kinematic fit is performed in which the $\gamma\gamma$ invariant mass is constrained to the known π^0 mass [21], and the χ^2 of the fit is required to be less than 50. The four-momentum of the π^0 candidate returned by this kinematic fit is used in the subsequent analyses.

To distinguish the ST D^- mesons from combinatorial backgrounds, we define the energy difference $\Delta E \equiv E_{D^-} - E_{\text{beam}}$ and the beam-constrained mass $M_{\text{BC}} \equiv \sqrt{E_{\text{beam}}^2/c^4 - |\vec{p}_{D^-}|^2/c^2}$, where E_{beam} is the beam energy, and E_{D^-} and \vec{p}_{D^-} are the total energy and momentum of the ST D^- meson in the e^+e^- center-of-mass frame. If there is more than one D^- candidate for each ST mode, the one with the least $|\Delta E|$ is retained for the subsequent analysis. The ΔE requirements and ST efficiencies are summarized in Table 1.

For each tag mode, the yield of ST D^- mesons is obtained by fitting the corresponding M_{BC} distribution. In the fit, the signal shape is described by MC-simulated signal shape convolved with a double-Gaussian function. The background shape is modeled by the ARGUS function [36], with the endpoint fixed at 1.8865 GeV/ c^2 corresponding to E_{beam} . Figure 2 shows the results of the fits to the M_{BC} distributions of the accepted ST candidates in data for different tag modes. The candidates with M_{BC} lying within $(1.863, 1.877)$ GeV/ c^2 for D^- tags are kept for the subsequent analysis. When summing over the tag modes the total yield of ST D^- mesons is determined to be $(4149.9 \pm 2.3_{\text{stat.}}) \times 10^3$.

5 DOUBLE-TAG SELECTION

The candidates for $D^+ \rightarrow K_S^0\pi^0e^+\nu_e$ decays are selected from the remaining tracks in the presence of the tagged D^- candidates. It is required that there are no extra good charged tracks ($N_{\text{extra}}^{\text{charge}}$) in addition to those used to construct the $D^+ \rightarrow K_S^0\pi^0e^+\nu_e$ candidate.

Candidates for K_S^0 and π^0 are selected with the same criteria as those used in the tag selection. The positron is identified using the TOF, dE/dx , and EMC measurements to

Table 1. The ΔE requirements, the measured ST D^- yields in the data (N_{ST}^i), the ST efficiencies (ϵ_{ST}^i) and DT efficiencies (ϵ_{DT}^i). The uncertainties are statistical only.

Tag mode	ΔE (GeV)	$N_{\text{ST}}^i (\times 10^3)$	ϵ_{ST}^i (%)	ϵ_{DT}^i (%)
$D^- \rightarrow K^+ \pi^- \pi^-$	(-0.025, 0.024)	2164.0 ± 1.5	51.17 ± 0.01	8.55 ± 0.01
$D^- \rightarrow K_S^0 \pi^-$	(-0.025, 0.026)	250.4 ± 0.5	50.74 ± 0.02	8.45 ± 0.03
$D^- \rightarrow K^+ \pi^- \pi^- \pi^0$	(-0.057, 0.046)	689.0 ± 1.1	25.50 ± 0.01	3.71 ± 0.01
$D^- \rightarrow K_S^0 \pi^- \pi^0$	(-0.062, 0.049)	558.4 ± 0.9	26.28 ± 0.01	3.92 ± 0.01
$D^- \rightarrow K_S^0 \pi^- \pi^- \pi^+$	(-0.028, 0.027)	300.5 ± 0.6	29.01 ± 0.01	4.23 ± 0.02
$D^- \rightarrow K^+ K^- \pi^-$	(-0.024, 0.023)	187.3 ± 0.5	41.06 ± 0.02	6.89 ± 0.03

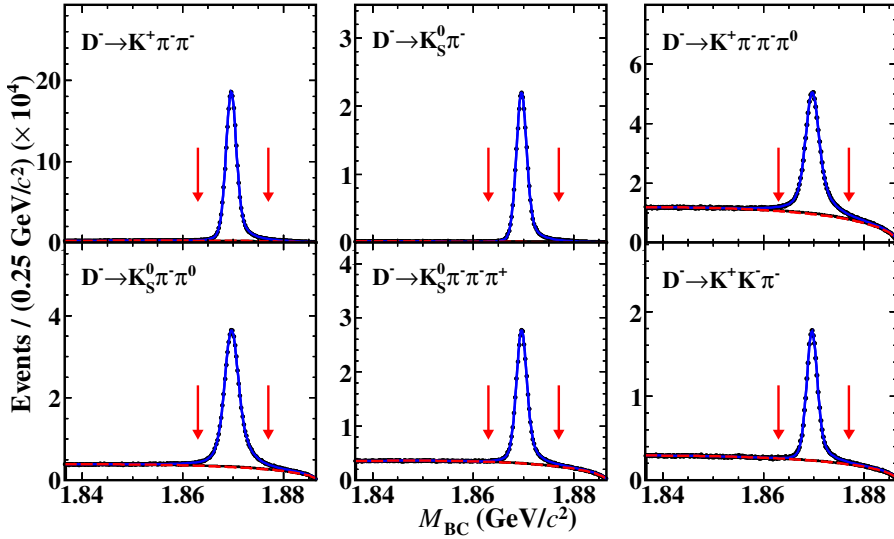


Figure 2. Fits to the M_{BC} distributions of the ST D^- candidates. In each plot, the points with error bars are data, the blue curves are the best fits, and the red dashed curves are the fitted combinatorial-background shapes. The pairs of red arrows show the M_{BC} signal windows.

calculate the combined confidence levels CL_e , CL_K , and CL_π for electron, kaon and pion hypotheses, respectively. The positron candidate is required to satisfy $CL_e > 0.8 \times (CL_e + CL_\pi + CL_K)$, $CL_e > 0.001$, and $E_{\text{EMC}}/p_{\text{MDC}} > 0.8c$. Here, E_{EMC} is the energy deposited in the EMC, while p_{MDC} is the momentum measured by the MDC.

To reject the backgrounds from hadronic decays involving a π^0 , such as $D^+ \rightarrow K_S^0 \pi^0 \pi^+ \pi^0$, the maximum energy of any extra photons ($E_{\text{extra } \gamma}^{\text{max}}$) which has not been used in the event selection is required to be less than 0.25 GeV for the $D^+ \rightarrow K_S^0 \pi^0 e^+ \nu_e$ selection. To suppress possible contamination from the hadronic decays $D^+ \rightarrow K_S^0 \pi^0 \pi^+$, where the pion is misidentified as a positron, the invariant mass of $K_S^0 \pi^0 e^+$ ($M_{K_S^0 \pi^0 e^+}$) is required to be less than 1.76 GeV/ c^2 . To suppress background events $D^+ \rightarrow K_S^0 e^+ \nu_e$ due to an additional fake π^0 , a new variable $U_{\text{miss}}^{K_S^0 e^+ \nu_e}$ is used. This variable is defined as $U_{\text{miss}}^{K_S^0 e^+ \nu_e} \equiv E_{\text{miss}}^{K_S^0 e^+ \nu_e} - p_{\text{miss}}^{K_S^0 e^+ \nu_e} c$, where $E_{\text{miss}}^{K_S^0 e^+ \nu_e} = E_{\text{beam}} - E_{K_S^0} - E_{e^+}$ and $p_{\text{miss}}^{K_S^0 e^+ \nu_e} = |\vec{p}_D - \vec{p}_{K_S^0} - \vec{p}_{e^+}|$. Here, $E_{\text{miss}}^{K_S^0 e^+ \nu_e}$ and

$p_{\text{miss}}^{K_S^0 e^+ \nu_e}$ represent the total energy and the momentum of all missing particles in the DT events, respectively. $U_{\text{miss}}^{K_S^0 e^+ \nu_e}$ is required to be larger than 0.04 GeV. These requirements have been optimized using a Figure of Merit defined as $\frac{S}{\sqrt{S+B}}$. Here, S and B denote the signal and background yields from the normalized inclusive MC sample.

The neutrino cannot be directly detected by the BESIII detector. To select semileptonic signal candidates, we define $U_{\text{miss}} \equiv E_{\text{miss}} - |\vec{p}_{\text{miss}}|c$, where E_{miss} and \vec{p}_{miss} are the missing energy and momentum, respectively, of the DT event in the e^+e^- center-of-mass frame. These quantities are calculated by $E_{\text{miss}} \equiv E_{\text{beam}} - E_{K_S^0} - E_{\pi^0} - E_{e^+}$ and $\vec{p}_{\text{miss}} \equiv \vec{p}_{D^+} - \vec{p}_{K_S^0} - \vec{p}_{\pi^0} - \vec{p}_{e^+}$, where $E_{K_S^0}(\pi^0)(e^+)$ and $\vec{p}_{K_S^0}(\pi^0)(e^+)$ are the measured energies and momenta of the $K_S^0(\pi^0)(e^+)$ candidates, respectively, and $\vec{p}_{D^+} \equiv -\hat{p}_{D^-} \sqrt{E_{\text{beam}}^2/c^2 - m_{D^-}^2}$, where \hat{p}_{D^-} is the unit vector in the momentum direction of the ST D^- meson and m_{D^-} is the nominal D^- mass [21]. In the presence of the ST D^- mesons, the average signal efficiency for $D^+ \rightarrow K_S^0 \pi^0 e^+ \nu_e$ is determined to be $(15.40 \pm 0.01)\%$, which is corrected according to the discussions in Sec. 7.

6 BRANCHING FRACTION

To extract the signal yield, an unbinned extended maximum-likelihood fit is performed to the U_{miss} distribution of the accepted candidates for $D^+ \rightarrow K_S^0 \pi^0 e^+ \nu_e$. In the fit, the signal shape is described by the MC-simulated shape convolved with a Gaussian function with floating parameters to account for the difference in resolution between data and MC simulation. The background shape is derived from the inclusive MC sample. The numbers of signal and background events are free parameters in the fit. The signal yields are determined to be (3852 ± 75) by fitting the U_{miss} distribution in data, and the fitting result is shown in Fig. 3. With Eq. (3.1), the BF of $D^+ \rightarrow K_S^0 \pi^0 e^+ \nu_e$ is determined to be $(0.881 \pm 0.017_{\text{stat.}} \pm 0.016_{\text{syst.}})\%$.

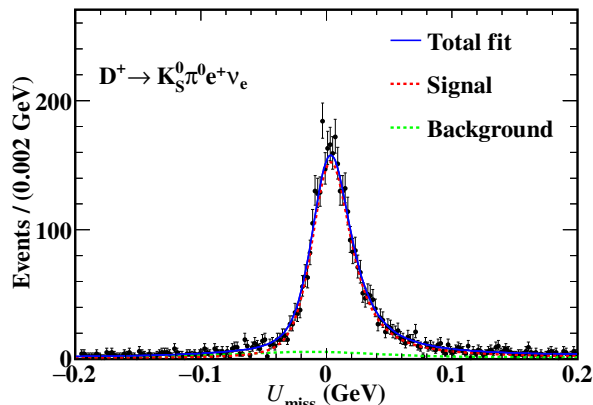


Figure 3. Fit to the U_{miss} distribution of the selected $D^+ \rightarrow K_S^0 \pi^0 e^+ \nu_e$ candidate events.

7 SYSTEMATIC UNCERTAINTY OF BRANCHING FRACTION

The DT method has the benefit that many systematic uncertainties due to the ST selection cancel in the ratio used to perform the BF measurement. Those systematic uncertainties that do not cancel, and those associated with the DT selection, are discussed below.

- (a) $N_{\text{ST}}^{\text{tot}}$: The uncertainty related to the ST yield $N_{\text{ST}}^{\text{tot}}$ is assigned to be 0.1% by varying the signal and background shapes. The signal shape is varied by changing the truth-matched angle from 15° to 10° or 20° , while the background shape is varied by changing the endpoint of ARGUS function from 1.8865 to 1.8863 or 1.8867 GeV/ c^2 . Additionally, the parameters of one of the two Gaussian functions used in the signal description is left free in the fit. Different fits are then performed of the M_{BC} distribution for each ST mode for both data and inclusive MC sample, and the difference in $N_{\text{ST}}/\epsilon_{\text{ST}}$ is assigned as the systematic uncertainty.
- (b) e^\pm tracking, PID and $E_{\text{EMC}}/p_{\text{MDC}}$: The systematic uncertainties arising from the knowledge of the tracking, PID efficiencies of e^\pm , and $E_{\text{EMC}}/p_{\text{MDC}}$ are assessed from a control sample of radiative Bhabha scattering events. The difference of the selection efficiency between data and MC simulation, 0.5%, is assigned as the corresponding systematic uncertainty.
- (c) K_S^0 reconstruction: The systematic uncertainty of the $K_S^0 \rightarrow \pi^+\pi^-$ reconstruction is considered to have two contributions. The π^\pm tracking efficiencies are evaluated using control samples of $D^0 \rightarrow K^-\pi^+$, $K^-\pi^+\pi^+\pi^-$ vs. $\bar{D}^0 \rightarrow K^+\pi^-$, $K^+\pi^-\pi^-\pi^+$, and $D^+ \rightarrow K^-\pi^+\pi^+$ vs. $D^- \rightarrow K^+\pi^-\pi^-\pi^-$ events. The event is fully reconstructed with the exception of one pion, the presence of which is inferred from the magnitude of the missing invariant mass in the event. The tracking efficiency is then measured directly by checking whether this pion is reconstructed. The difference in π^\pm tracking efficiencies between data and MC simulation is determined. The efficiencies associated with the K_S^0 mass window, primary vertex and K_S^0 decay vertex fit are studied in hadronic $D\bar{D}$ events, with D^0 decaying into $K_S^0\pi^+\pi^-$, $K_S^0\pi^+\pi^-\pi^0$ and $K_S^0\pi^0$, or D^+ decaying into $K_S^0\pi^+$, $K_S^0\pi^+\pi^0$, and $K_S^0\pi^+\pi^+\pi^-$. After correcting the MC efficiencies to the data, the residual statistical uncertainties of the data/MC differences are assigned as the systematic uncertainties.
- (d) π^0 reconstruction: The uncertainty from the π^0 reconstruction is assigned to be 1.0% after studying a control sample of $D^0 \rightarrow K^-\pi^+\pi^0$ decays. The difference between data and MC simulation is $(99.4 \pm 1.0)\%$. After correcting the MC efficiencies to data, we assign 1.0% as the uncertainty for π^0 reconstruction.
- (e) Assumed \mathcal{B} : The uncertainties in the assumed BFs of $K_S^0 \rightarrow \pi^+\pi^-$ and $\pi^0 \rightarrow \gamma\gamma$ are 0.07% and 0.03% [21], respectively.
- (f) MC sample size: The uncertainty due to the MC sample size is 0.1%.

- (g) $E_{\text{extra}\gamma}^{\text{max}}$ and $N_{\text{charge}}^{\text{good}}$ requirements: The systematic uncertainty from the $E_{\text{extra}\gamma}^{\text{max}}$ and $N_{\text{charge}}^{\text{good}}$ requirements is estimated to be 0.8%, after performing DT samples of $D^+ \rightarrow K_S^0 e^+ \nu_e$ decays versus the tag modes, reconstructed as in the baseline analysis.
- (h) $M_{K_S^0 \pi^0 e^+}$ requirement: The uncertainty associated with the $M_{K_S^0 \pi^0 e^+}$ requirement is studied by varying its value by $\pm 10 \text{ MeV}/c^2$, following the method defined in Refs. [37–39]. The maximum change in the signal efficiency is taken as the associated systematic uncertainty.
- (i) $U_{\text{miss}}^{K_S^0 e^+ \nu_e}$ requirement: The efficiencies of the $U_{\text{miss}}^{K_S^0 e^+ \nu_e}$ requirement are greater than 99% and the difference of these efficiencies between data and MC simulation is negligible.
- (j) MC model: The signal MC samples in this study are generated with the generator developed with the parameters obtained in Section. 8. New MC samples are generated in which the input form factors r_V and r_2 are varied by $\pm 1\sigma$ of their statistical uncertainty around their baseline values. The largest change in the signal efficiency, 1.0%, is taken as the systematic uncertainty in the MC generator.

The total systematic uncertainty is obtained by adding the individual components in quadrature (δ_{sys}), assuming that all sources are independent of each other. Table 2 summarizes the sources of the systematic uncertainties in the BF measurement.

Table 2. Relative systematic uncertainties (in %) in the BF measurement.

Source	Uncertainty
$N_{\text{ST}}^{\text{tot}}$	0.1
e^\pm tracking	0.5
e^\pm PID and $E_{\text{EMC}}/p_{\text{MDC}}$	0.5
K_S^0 reconstruction	1.0
π^0 reconstruction	1.0
Assumed \mathcal{B}	0.1
MC samples size	0.1
$E_{\text{extra}\gamma}^{\text{max}}$ & $N_{\text{charge}}^{\text{good}}$ requirements	0.8
$M_{K_S^0 \pi^0 e^+}$ requirement	0.2
$U_{\text{miss}}^{K_S^0 e^+ \nu_e}$ requirement	negligible
MC model	1.0
Total	2.1

8 AMPLITUDE ANALYSIS OF $D^+ \rightarrow K_S^0 \pi^0 e^+ \nu_e$

To prepare a sample for the study of the decay dynamics of $D^+ \rightarrow K_S^0 \pi^0 e^+ \nu_e$, an additional requirement of $U_{\text{miss}} \in [-0.04, 0.06] \text{ GeV}$ is imposed on the events selected for the branching-fraction measurement. With this additional requirement, we observe 3566

candidates in data with a background fraction of $(6.54 \pm 0.64)\%$. The four-body decay $D^+ \rightarrow K_S^0 \pi^0 e^+ \nu_e$ can be uniquely characterized by five kinematic variables [40, 41], as illustrated in Fig. 4: the invariant-mass squared of $K_S^0 \pi^0$ (m^2), the invariant-mass squared of $e^+ \nu_e$ (q^2), the angle between the three-momentum of the K_S^0 in the $K_S^0 \pi^0$ rest frame and the direction of flight of the $K_S^0 \pi^0$ in the D^+ rest frame ($\theta_{K_S^0}$), the angle between the three-momentum of e^+ in the $e^+ \nu_e$ rest frame and the direction of flight of the $e^+ \nu_e$ in the D^+ rest frame (θ_e), and the angle between the two decay planes (χ). The sign of χ is changed when analyzing D^- decays to ensure CP conservation. Neglecting the mass of the positron, the differential decay width for the $D^+ \rightarrow K_S^0 \pi^0 e^+ \nu_e$ decay is written as [42]

$$d^5\Gamma = \frac{G_F^2 |V_{cs}|^2}{(4\pi)^6 m_D^3} X \beta \mathcal{I}(m^2, q^2, \theta_{K_S^0}, \theta_e, \chi) \times dm^2 dq^2 d\cos(\theta_{K_S^0}) d\cos(\theta_e) d\chi. \quad (8.1)$$

In this expression, G_F is the Fermi constant, $|V_{cs}|$ is the $c \rightarrow s$ CKM matrix element, $X = p_{K_S^0 \pi^0} m_{D^+}$, where $p_{K_S^0 \pi^0}$ is the momentum of $K_S^0 \pi^0$ in the D^+ rest frame, and $\beta = 2p^*/m$, where p^* denotes the momentum of K_S^0 in the $K_S^0 \pi^0$ rest frame. The dependence of \mathcal{I} on θ_e and χ is given by [42]

$$\begin{aligned} \mathcal{I} = & \mathcal{I}_1 + \mathcal{I}_2 \cos 2\theta_e + \mathcal{I}_3 \sin^2 \theta_e \cos 2\chi + \mathcal{I}_4 \sin 2\theta_e \cos \chi + \\ & \mathcal{I}_5 \sin \theta_e \cos \chi + \mathcal{I}_6 \cos \theta_e + \mathcal{I}_7 \sin \theta_e \sin \chi + \mathcal{I}_8 \sin 2\theta_e \sin \chi + \mathcal{I}_9 \sin^2 \theta_e \sin 2\chi, \end{aligned} \quad (8.2)$$

where the quantities $\mathcal{I}_{1,\dots,9}$ depend on m^2 , q^2 , and $\theta_{K_S^0}$. These quantities can be expressed in terms of three form factors $\mathcal{F}_{1,2,3}$:

$$\begin{aligned} \mathcal{I}_1 &= \frac{1}{4} \{ |\mathcal{F}_1|^2 + \frac{3}{2} \sin^2 \theta_{K_S^0} (|\mathcal{F}_2|^2 + |\mathcal{F}_3|^2) \}, \\ \mathcal{I}_2 &= -\frac{1}{4} \{ |\mathcal{F}_1|^2 - \frac{1}{2} \sin^2 \theta_{K_S^0} (|\mathcal{F}_2|^2 + |\mathcal{F}_3|^2) \}, \\ \mathcal{I}_3 &= -\frac{1}{4} \{ |\mathcal{F}_2|^2 - |\mathcal{F}_3|^2 \} \sin^2 \theta_{K_S^0}, \\ \mathcal{I}_4 &= \frac{1}{2} \text{Re}(\mathcal{F}_1^* \mathcal{F}_2) \sin \theta_{K_S^0}, \\ \mathcal{I}_5 &= \text{Re}(\mathcal{F}_1^* \mathcal{F}_3) \sin \theta_{K_S^0}, \\ \mathcal{I}_6 &= \text{Re}(\mathcal{F}_2^* \mathcal{F}_3) \sin^2 \theta_{K_S^0}, \\ \mathcal{I}_7 &= \text{Im}(\mathcal{F}_1 \mathcal{F}_2^*) \sin \theta_{K_S^0}, \\ \mathcal{I}_8 &= \frac{1}{2} \text{Im}(\mathcal{F}_1 \mathcal{F}_3^*) \sin \theta_{K_S^0}, \\ \mathcal{I}_9 &= -\frac{1}{2} \text{Im}(\mathcal{F}_2 \mathcal{F}_3^*) \sin^2 \theta_{K_S^0}. \end{aligned} \quad (8.3)$$

The form factors \mathcal{F}_i can be expanded into partial waves to show their explicit dependence on $\theta_{K_S^0}$. In this analysis, we only consider S and P waves, and thereby obtain

$$\begin{aligned}\mathcal{F}_1 &= \mathcal{F}_{1S} + \mathcal{F}_{1P} \cos \theta_{K_S^0}, \\ \mathcal{F}_2 &= \frac{1}{\sqrt{2}} \mathcal{F}_{2P}, \\ \mathcal{F}_3 &= \frac{1}{\sqrt{2}} \mathcal{F}_{3P}.\end{aligned}\tag{8.4}$$

Here, \mathcal{F}_{iS} and \mathcal{F}_{iP} correspond to S and P waves.

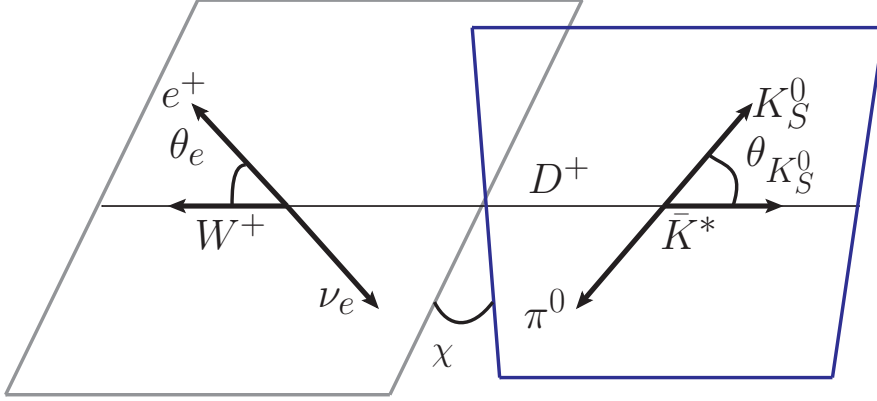


Figure 4. Definition of the angular variables in the $D^+ \rightarrow K_S^0 \pi^0 e^+ \nu_e$ decay.

8.1 S-WAVE FORM FACTOR

The S -wave related form-factor F_{1S} is expressed as

$$F_{10} = p_{K_S^0 \pi^0} m_D \frac{1}{1 - \frac{q^2}{m_A^2}} \mathcal{A}_S(m).\tag{8.5}$$

The S -wave amplitude $\mathcal{A}_S(m)$ is considered to be the superposition of a non-resonant background and the $\bar{K}_0^*(1430)$ resonance. The phase parameterization used for the S -wave amplitude, as proposed by the LASS collaboration [44], is given by

$$\cot(\delta_{BG}^{1/2}) = \frac{1}{a_{S,BG}^{1/2} p^*} + \frac{b_{S,BG}^{1/2} p^*}{2},\tag{8.6}$$

$$\cot(\delta_{\bar{K}_0^*(1430)}^{1/2}) = \frac{m_{\bar{K}_0^*(1430)}^2 - m^2}{m_{\bar{K}_0^*(1430)} \Gamma_{\bar{K}_0^*(1430)}(m)},\tag{8.7}$$

$$\delta(m) = \delta_{BG}^{1/2} + \delta_{\bar{K}_0^*(1430)}^{1/2},\tag{8.8}$$

where $\delta_{BG}^{1/2}$ is the scattering length determined by the fit, $b_{S,BG}^{1/2}$ is the effective range fixed at -0.81 [20], and $\delta_{\bar{K}_0^*(1430)}^{1/2}$ is the total phase of the S wave.

The amplitude $\mathcal{A}_S(m)$ is described with formalism developed by the BaBar collaboration [19]. It is constructed as a piecewise function for m below and above the $\mathcal{A}_S(m)$ pole-mass value:

$$\mathcal{A}_S(m) = r_S P(m) e^{i\delta(m)}, m < m_{\bar{K}_0^*(1430)}; \quad (8.9)$$

$$\mathcal{A}_S(m) = r_S P(m_{\bar{K}_0^*(1430)}) \times e^{i\delta(m)} \sqrt{\frac{(m_{\bar{K}_0^*(1430)} \Gamma_{\bar{K}_0^*(1430)})^2}{(m_{\bar{K}_0^*(1430)}^2 - m^2)^2 + (m_{\bar{K}_0^*(1430)} \Gamma_{\bar{K}_0^*(1430)})^2}}, m > m_{\bar{K}_0^*(1430)}. \quad (8.10)$$

In these expressions, $P(m) = 1 + r_S^{(1)} x$, $x = \sqrt{\left(\frac{m}{m_{K_S^0} + m_{\pi^0}}\right) - 1}$. r_S is a dimensionless parameter, and the parameter $r_S^{(1)}$ represents the relative strength of the S wave, and $e^{i\delta(m)}$ introduces an overall phase to the S wave. The magnitude is assumed to have a linear variation versus m below the pole while behaving according to the Breit-Wigner function above the pole.

8.2 P-WAVE FORM FACTOR

The P -wave related form-factors \mathcal{F}_{iP} can be parameterized by the helicity form-factors $H_{0,\pm}$. These form factors are given by

$$\begin{aligned} \mathcal{F}_{1P} &= 2\sqrt{2}\alpha q H_0 \times \mathcal{A}(m), \\ \mathcal{F}_{2P} &= 2\alpha q (H_+ + H_-) \times \mathcal{A}(m), \\ \mathcal{F}_{3P} &= 2\alpha q (H_+ - H_-) \times \mathcal{A}(m). \end{aligned} \quad (8.11)$$

Here, the α value depends on the definition of the P -wave amplitude $\mathcal{A}(m)$, as shown in Eq. (8.18). The helicity form-factors, related to two axial-vector form-factors $A_{1,2}(q^2)$ and one vector form-factor $V(q^2)$, are given by

$$\begin{aligned} H_0(q^2) &= \frac{1}{2mq} [(m_D^2 - m^2 - q^2)(m_D + m)A_1(q^2) - 4\frac{m_D^2 p_{K_S^0 \pi^0}^2}{m_D + m} A_2(q^2)], \\ H_{\pm}(q^2) &= [(m_D + m)A_1(q^2) \mp \frac{2m_D p_{K_S^0 \pi^0}}{(m_D + m)} V(q^2)]. \end{aligned} \quad (8.12)$$

The q^2 dependence is described using a single-pole dominance parametrization [45–47], which is written as

$$\begin{aligned} V(q^2) &= \frac{V(0)}{1 - \frac{q^2}{m_V^2}}, \\ A_1(q^2) &= \frac{A_1(0)}{1 - \frac{q^2}{m_A^2}}, \\ A_2(q^2) &= \frac{A_2(0)}{1 - \frac{q^2}{m_A^2}}. \end{aligned} \quad (8.13)$$

The pole masses m_V and m_A are fixed at $1.81\text{GeV}/c^2$ and $2.61\text{ GeV}/c^2$ [20], respectively. The ratios of the form factors taken at $q^2 = 0$, $r_V = V(0)/A_1(0)$ and $r_2 = A_2(0)/A_1(0)$, can reflect the variation of the differential decay rate versus the kinematic variables. They are determined by the fit to the data. The P -wave amplitude $\mathcal{A}(m)$ is defined as

$$\mathcal{A}(m) = \frac{m_0 \Gamma_0 F_J(m)}{m_0^2 - m^2 - im_0 \Gamma(m)}, \quad (8.14)$$

where m_0 and Γ_0 are the pole mass and the total width of $\bar{K}^*(892)^0$, respectively. The width $\Gamma(m)$ is given by

$$\Gamma(m) = \Gamma_0 \frac{p^* m_0}{p_0^* m} F_J^2(m), \quad (8.15)$$

$$F_J = \left(\frac{p^*}{p_0^*}\right)^J \frac{B_J(p^*)}{B_J(p_0^*)}, \quad (8.16)$$

where B_J is the Blatt-Weisskopf damping factor [43]. In this case $J = 1$ and

$$B_1 = 1/\sqrt{1 + r_{BW}^2 p^{*2}}. \quad (8.17)$$

Here, the p^* is the momentum of the K_S^0 in the $K_S^0 \pi^0$ rest frame, and p_0^* is the value taken at the pole mass of the resonance. A common value of r_{BW} for light mesons is about 0.5 fm, so it is fixed at 3.07 GeV^{-1} in natural units [20].

The factor α entering in Eq. (8.11) is equal to

$$\alpha = \sqrt{\frac{3\pi \mathcal{B}_{\bar{K}^*(892)^0}}{p_0^* \Gamma_0}}, \quad (8.18)$$

where $\mathcal{B}_{\bar{K}^*(892)^0} = \mathcal{B}(\bar{K}^*(892)^0 \rightarrow \bar{K}^0 \pi^0)$.

8.3 AMPLITUDE-ANALYSIS METHOD

We utilize the unbinned maximum-likelihood method within the RooFit [48] framework to perform the amplitude-analysis fit. The probability density function (PDF) for a single candidate event is given by

$$\text{PDF}(\xi, \eta) = \frac{\omega(\xi, \eta) \epsilon(\xi) R_4(\xi)}{\int d\xi \omega(\xi, \eta) R_4(\xi) \epsilon(\xi)}, \quad (8.19)$$

where ξ is the final state of the event, and η corresponds to the fit parameters in the PDF. Here, $\omega(\xi, \eta)$ denotes the decay intensity (as defined in Eq. (8.2)), $\epsilon(\xi)$ is the reconstruction efficiency for the final state ξ , and $R_4(\xi)$ is the phase space factor.

The likelihood is expressed as the product of probabilities for all N events. It is given by

$$\mathcal{L} = \prod_{i=1}^N \text{PDF}(\xi_i, \eta) = \prod_{i=1}^N \frac{\omega(\xi_i, \eta) \epsilon(\xi_i) R_4(\xi_i)}{\int d\xi_i \omega(\xi_i, \eta) R_4(\xi_i) \epsilon(\xi_i)}. \quad (8.20)$$

During the fitting process, the parameters η are optimized by minimizing the negative log-likelihood (NLL), which is written as

$$-\ln\mathcal{L} = -\sum_{i=1}^N \ln(\epsilon(\xi_i)R_4(\xi_i)) - \sum_{i=1}^N \ln \frac{\omega(\xi_i, \eta)}{\int d\xi_i \omega(\xi_i, \eta) R_4(\xi_i) \epsilon(\xi_i)}. \quad (8.21)$$

The first term in the above equation depends only on the efficiency, and remains constant throughout the fit. Therefore, only the computation of the second term is performed in the fit. The NLL to be minimized can therefore be written as

$$\text{NLL} = -\sum_{i=1}^N \ln \frac{\omega(\xi_i, \eta)}{\sigma}, \quad (8.22)$$

where $\sigma = \int d\xi_i \omega(\xi_i, \eta) R_4(\xi_i) \epsilon(\xi_i)$.

The acceptance efficiency is taken into account in the calculation of the cross section σ , which is determined through MC integration with the signal MC sample [49]. Initially, we use phase space (PHSP) MC samples with the uniform distribution of the kinematics to obtain the cross section σ . After obtaining the first set of solutions in the amplitude analysis, we update σ from MC samples generated with this new set of solutions, and iterate until the solution stabilizes. The normalization integral term is given as

$$\sigma = \int \omega(\xi, \eta) \epsilon(\xi) R_4(\xi) d\xi \propto \frac{1}{N_{\text{selected}}} \sum_{k=1}^{N_{\text{selected}}} \frac{\omega(\xi_k, \eta)}{\omega(\xi_k, \eta_0)}. \quad (8.23)$$

Here, the terms η and η_0 are the values of the parameters used in the fit and that used to produce the simulated events, respectively. N_{selected} denotes the number of the signal MC events after reconstruction and selection.

The background is estimated using the inclusive MC sample. It is subtracted from the total one via

$$\text{NLL} = (-\ln L_{\text{total}} - \omega(-\ln L_{\text{background}})), \quad (8.24)$$

where ω is a normalization factor of the inclusive MC sample corresponding to the data size, with a value of 0.0185.

The goodness of the fit is estimated using $\chi^2/\text{n.d.f.}$, where n.d.f. denotes the number of degrees of freedom. The χ^2 is calculated by comparing the distribution in the five kinematic variables between data and the MC sample, determined by the results of the amplitude analysis. The χ^2 value is determined by

$$\chi^2 = \sum_i^{N_{\text{bin}}} \frac{(n_i^{\text{data}} - n_i^{\text{fit}})^2}{n_i^{\text{fit}}}. \quad (8.25)$$

Based on the amplitude analysis solution, we calculate the fractions of each component according to $f_k = \frac{\int d\xi \omega_k(\xi, \eta)}{\int d\xi \omega(\xi, \eta)}$, which represents the ratio of the decay intensity of the specific component to the total intensity. The $\omega_k(\xi, \eta)$ and $\omega(\xi, \eta)$ are the decay intensities of the

k -th component and the total amplitude, respectively. In our analysis, we employ a large PHSP MC sample of 4×10^6 events, without considering detector acceptance or resolution effects. To estimate the statistical uncertainty of the fraction, the fit results are iteratively adjusted based on the error covariance matrix of the fit, and new fractions are computed. Comparisons of the projections over the five kinematic variables between data and the amplitude analysis solution are illustrated in Fig. 5. The fit results are summarized in Table 3.

Table 3. The fitted parameters of the amplitude model under the assumption that the signal is composed of S -wave and $\bar{K}^*(892)^0$ components. The first and second uncertainties are statistical and systematic, respectively.

Variable	Value
r_2	$0.72 \pm 0.06 \pm 0.02$
r_V	$1.43 \pm 0.07 \pm 0.03$
$a_{S,BG}^{1/2}$ (GeV/ c) ⁻¹	$2.04 \pm 0.17 \pm 0.17$
$m_{\bar{K}^*(892)^0}$ (MeV/ c^2)	$893.82 \pm 0.57 \pm 0.11$
r_S (GeV) ⁻¹	$-8.34 \pm 0.24 \pm 0.30$
$\Gamma_{\bar{K}^*(892)^0}^0$ (MeV/ c^2)	$46.46 \pm 1.15 \pm 0.70$
$f_{S\text{-wave}}$	$6.13 \pm 0.27 \pm 0.30$
$f_{\bar{K}^*(892)^0}$	$93.88 \pm 0.27 \pm 0.29$

8.4 SYSTEMATIC UNCERTAINTY OF AMPLITUDE ANALYSIS

The systematic uncertainties in the amplitude analysis are discussed below.

- (a) Background estimation: The uncertainties associated with the background contribution are studied by varying the fraction of the background events within its statistical uncertainty. The differences in fit result for each parameter are assigned as the corresponding systematic uncertainties.
- (b) $r_S^{(1)}$, $b_{S,BG}^{1/2}$, and r_{BW} : The uncertainties from the fixed parameters are estimated by varying the input values by $\pm 1\sigma$ [20] and re-performing the fit. The largest difference is taken as the systematic uncertainty due to the imperfect knowledge of each parameter.
- (c) m_V and m_A : The systematic uncertainties associated with the pole-mass assumption are estimated by varying m_V and m_A by ± 50 MeV/ c^2 . [20]. The resulting differences compared to the baseline-fit solution are taken as the corresponding systematic uncertainties.
- (d) Fit bias: The possibility of bias in the fit procedure is assessed by inspecting pull distributions from fits to 300 MC samples with a size equal to the data, where these samples considered detector acceptance and resolution effects. The means of the pulls are compatible with zero in all cases, but the widths are greater than unity by 10–20% for certain parameters. The statistical uncertainties of these parameters are scaled to reflect these slightly wider than expected pulls.

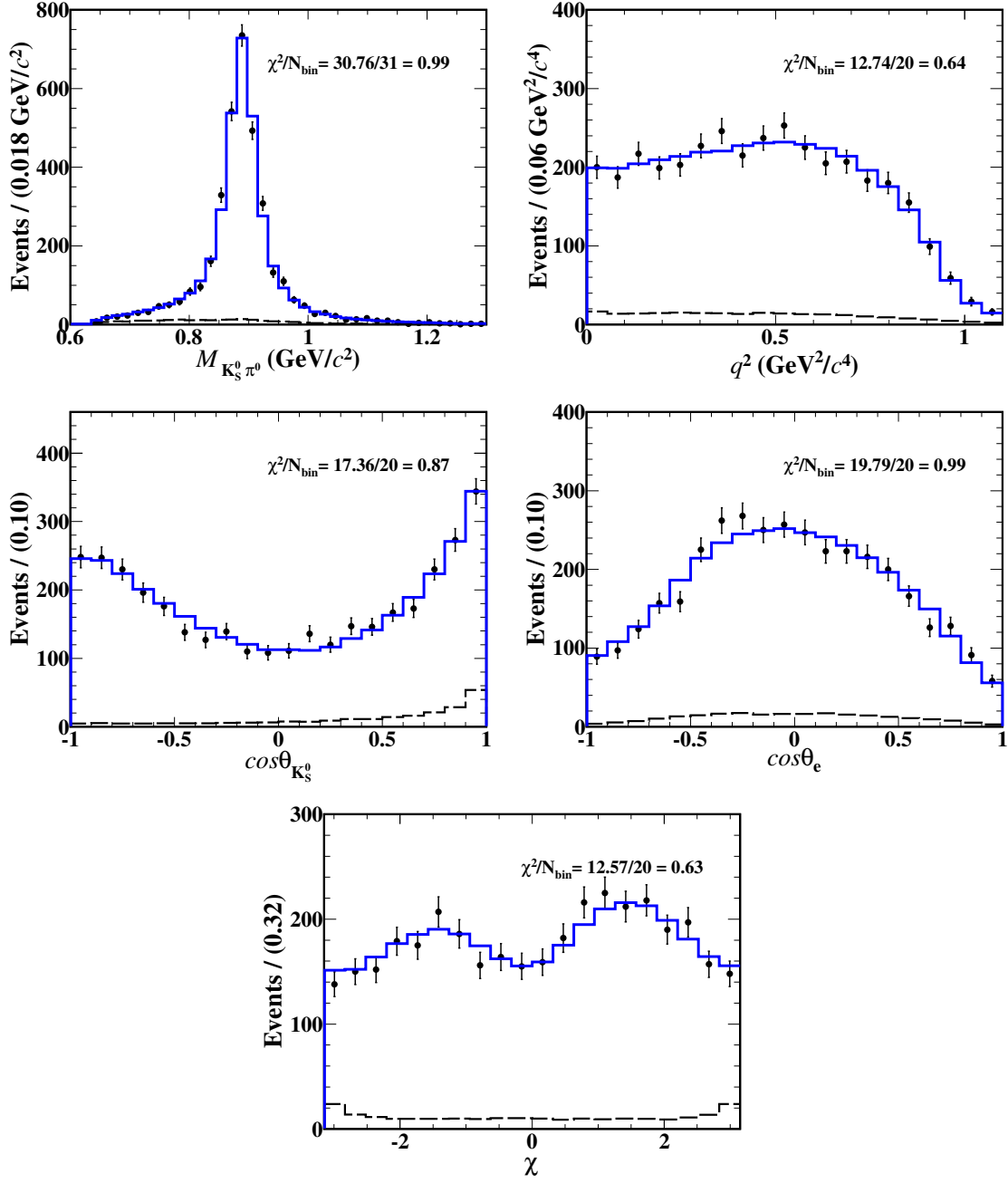


Figure 5. Projections of the data and simultaneous amplitude analysis fit onto five kinematic variables for $D^+ \rightarrow K_S^0 \pi^0 e^+ \nu_e$. The dots with error bars are data, the blue lines are the best fit, and the dashed lines show the sum of the simulated backgrounds. For the χ^2/N_{bin} calculation, we merge any neighboring bins with very few entries until there are 10 entries accumulated.

Assuming that all sources are independent, the total systematic uncertainties on the amplitude analysis are determined by adding all uncertainties in quadrature. The component systematic uncertainties and the totals are summarized in Table 4.

Table 4. The systematic uncertainties on the fitted parameters in the amplitude analysis (in %).

Source	Δr_2	Δr_V	$\Delta a_{S,BG}^{1/2}$	$\Delta m_{\bar{K}^*(892)^0}$	Δr_S	$\Delta \Gamma_{\bar{K}^*(892)^0}^0$	$\Delta f_{\bar{K}^*(892)^0}$	$\Delta f_{S\text{-wave}}$
Background estimation	0.8	0.1	0.4	0.002	0.4	1.1	0.1	1.1
$r_S^{(1)}$	0.7	1.1	0.4	0.005	3.1	0.4	0.2	3.4
$b_{S,BG}^{1/2}$	1.3	0.2	8.0	0.004	0.5	0.4	0.1	0.8
r_{BW}	1.4	0.6	1.0	0.008	1.8	0.8	0.2	3.1
m_V	1.1	1.6	0.2	0.005	0.1	0.2	0.0	0.4
m_A	1.5	0.5	0.4	0.004	0.2	0.2	0.0	0.2
Fit bias	–	–	–	–	–	–	–	–
Total	2.8	2.0	8.1	0.012	3.6	1.5	0.3	4.8

9 SUMMARY

Based on 7.93 fb^{-1} of e^+e^- collision data taken at $\sqrt{s} = 3.773 \text{ GeV}$, the BF of $D^+ \rightarrow K_S^0 \pi^0 e^+ \nu_e$ is measured for the first time and determined to be $\mathcal{B}(D^+ \rightarrow K_S^0 \pi^0 e^+ \nu_e) = (0.881 \pm 0.017_{\text{stat.}} \pm 0.016_{\text{syst.}})\%$. From the analysis of the $D^+ \rightarrow K_S^0 \pi^0 e^+ \nu_e$ decay dynamics, the S -wave and P -wave components are determined with fractions of $f_{S\text{-wave}} = (6.13 \pm 0.27_{\text{stat.}} \pm 0.30_{\text{syst.}})\%$, and $f_{\bar{K}^*(892)^0} = (93.88 \pm 0.27_{\text{stat.}} \pm 0.29_{\text{syst.}})\%$, respectively. From these results the BFs of the two components are calculated to be $\mathcal{B}(D^+ \rightarrow (K_S^0 \pi^0)_{S\text{-wave}} e^+ \nu_e) = (5.41 \pm 0.35_{\text{stat.}} \pm 0.37_{\text{syst.}}) \times 10^{-4}$ and $\mathcal{B}(D^+ \rightarrow \bar{K}^*(892)^0 e^+ \nu_e) = (4.97 \pm 0.11_{\text{stat.}} \pm 0.12_{\text{syst.}})\%$, where $\mathcal{B}(\bar{K}^*(892)^0 \rightarrow \bar{K}^0 \pi^0) \times \mathcal{B}(\bar{K}^0 \rightarrow K_S^0) = 1/6$ based on isospin conservation with negligible uncertainty. Additionally, the hadronic form-factor ratios of the $D^+ \rightarrow \bar{K}^*(892)^0 e^+ \nu_e$ decay are determined to be $r_V = 1.43 \pm 0.07_{\text{stat.}} \pm 0.03_{\text{syst.}}$ and $r_2 = 0.72 \pm 0.06_{\text{stat.}} \pm 0.02_{\text{syst.}}$. Figure 6 shows the comparisons of r_V and r_2 with different experimental results. Figure 7 shows the comparison of our BF of $D^+ \rightarrow \bar{K}^*(892)^0 e^+ \nu_e$ with other measurements. Our results are consistent with those reported in other experiments [17–20]. Table 5 shows the hadronic form factors of $D \rightarrow \bar{K}^*$ predicted by different theoretical calculations, as well as the values measured in the current study. The measured results of r_V and r_2 are consistent with several Lattice QCD calculations within 2σ [7–10, 12], but disfavor those that employ a large lattice spacing [11], as well as those predictions based on the quark model [13–15] and QCD sum rules [16].

Acknowledgments

The BESIII Collaboration thanks the staff of BEPCII and the IHEP computing center for their strong support. This work is supported in part by National Key R&D Program of China under Contracts Nos. 2023YFA1606000, 2020YFA0406300, 2020YFA0406400; National Natural Science Foundation of China (NSFC) under Contracts Nos. 11635010, 11735014, 11935015, 11935016, 11935018, 12025502, 12035009, 12035013, 12061131003, 12192260, 12192261, 12192262, 12192263, 12192264, 12192265, 12221005, 12225509, 12235017, 12361141819; Natural Science Foundation of Hunan Province (Contracts No.2024JJ2044); Guangdong Basic and Applied Basic Research Foundation under Grant No. 2023A1515010121 and the Fundamental Research Funds for the Central Universities under Contract No. 020400/531118010467; the Chinese Academy of Sciences (CAS) Large-Scale Scientific Fa-

Table 5. Hadronic form factors of $D \rightarrow \bar{K}^*$ at $q^2=0$ predicted by different theories.

Reference		r_V	r_2
Experiment	Average [21]	1.49 ± 0.05	0.802 ± 0.021
Lattice QCD	LMMS [7]	1.6 ± 0.2	0.4 ± 0.4
	BKS [8]	$1.99 \pm 0.22 \pm 0.33$	$0.7 \pm 0.16 \pm 0.17$
	ELC [9]	1.3 ± 0.2	0.6 ± 0.3
	UKQCD [10]	$1.4^{+0.5}_{-0.2}$	0.9 ± 0.2
	LANL [11]	1.83 ± 0.09	0.74 ± 0.19
	APE [12]	1.6 ± 0.3	0.7 ± 0.4
Quark model	WSB [13]	1.4	1.3
	ISGW [14]	1.4	1.0
	GS [15]	2.0	0.8
QCD sum rules	BBD [16]	2.2 ± 0.2	1.2 ± 0.2
This work	—	$1.43 \pm 0.07_{\text{stat.}} \pm 0.03_{\text{sys.}}$	$0.72 \pm 0.06_{\text{stat.}} \pm 0.02_{\text{sys.}}$

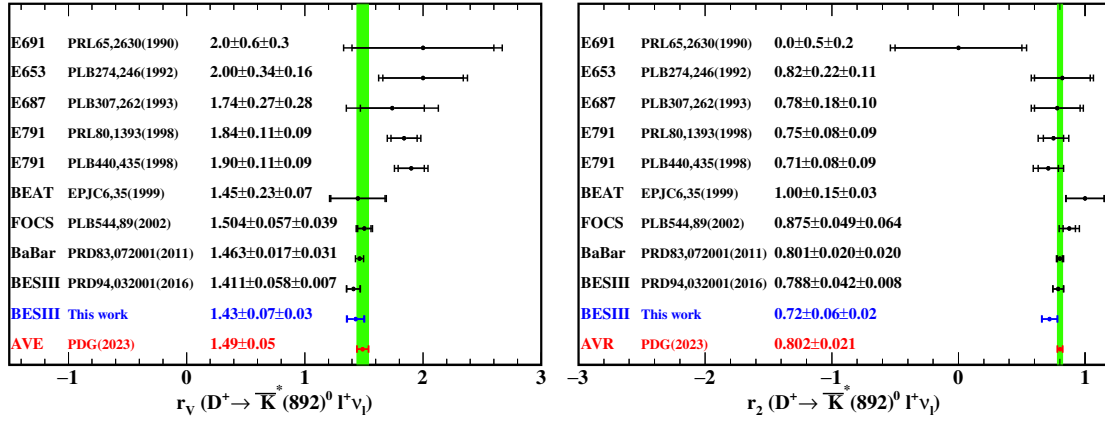


Figure 6. Comparison of r_V and r_2 with other measurements. The first and second uncertainties are statistical and systematic, respectively. The green band represents the average value in the PDG2023.

ility Program; the CAS Center for Excellence in Particle Physics (CCEPP); Joint Large-Scale Scientific Facility Funds of the NSFC and CAS under Contract No. U1832207; CAS Key Research Program of Frontier Sciences under Contracts Nos. QYZDJ-SSW-SLH003, QYZDJ-SSW-SLH040; 100 Talents Program of CAS; The Institute of Nuclear and Particle Physics (INPAC) and Shanghai Key Laboratory for Particle Physics and Cosmology; European Union’s Horizon 2020 research and innovation programme under Marie Skłodowska-Curie grant agreement under Contract No. 894790; German Research Foundation DFG under Contracts Nos. 455635585, Collaborative Research Center CRC 1044, FOR5327, GRK 2149; Istituto Nazionale di Fisica Nucleare, Italy; Ministry of Development of Turkey under Contract No. DPT2006K-120470; National Research Foundation of Korea under Contract No. NRF-2022R1A2C1092335; National Science and Technology Fund of Mongolia; National Science Research and Innovation Fund (NSRF) via the Program Management Unit for Human Resources & Institutional Development, Research and Innovation of Thailand under Contract No. B16F640076; Polish National Science Centre under Contract No.

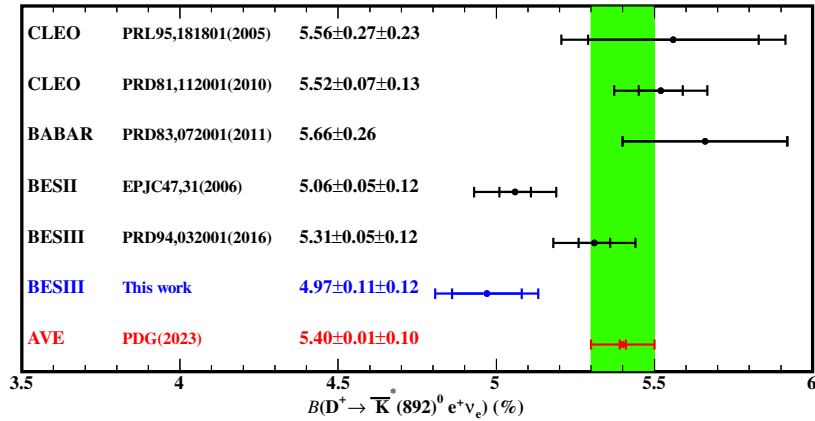


Figure 7. Comparison of our BF of $D^+ \rightarrow \bar{K}^*(892)^0 e^+ \nu_e$ with other measurements. The first and second uncertainties are statistical and systematic, respectively. The green band represents the average value in the PDG2023.

2019/35/O/ST2/02907; The Swedish Research Council; U. S. Department of Energy under Contract No. DE-FG02-05ER41374.

References

- [1] M. Antonelli *et al.*, *Flavor Physics in the Quark Sector*, *Phys. Rep.* **494** (2010) 197 [arXiv:hep-ex/0907.5386] [INSPIRE].
- [2] N. Isgur *et al.*, *Semileptonic Band D decays in the quark model*, *Phys. Rev.* **39** (1989) 799 [INSPIRE].
- [3] N. Isgur *et al.*, *Semileptonic meson decays in the quark model: An update*, *Phys. Rev.* **52** (1995) 2783 [arXiv:hep-ex/9503486] [INSPIRE].
- [4] N. Cabibbo, *Unitary Symmetry and Leptonic Decays*, *Phys. Rev. Lett.* **10** (1963) 531 [INSPIRE].
- [5] M. Kobayashi and T. Maskawa, *CP Violation in the Renormalizable Theory of Weak Interaction*, *Prog. Theor. Phys.* **49** (1973) 652 [INSPIRE].
- [6] B. C. Ke, J. Koponen, H. B. Li and Y. Zheng, *Recent Progress in Leptonic and Semileptonic Decays of Charmed Hadrons*, *Ann. Rev. Nucl. Part. Sci.* **73** (2023) 285 [arXiv:hep-ex/2310.05228] [INSPIRE].
- [7] V. Lubicz, G. Martinelli, M. S. McCarthy, and C. T. Sachrajda, *Semileptonic decays of D mesons in a lattice QCD*, *Phys. Lett. B* **274** (1992) 415 [INSPIRE].
- [8] C. W. Bernard, A. X. El-Khadra and A. Soni, *Lattice study of semileptonic decays of charm mesons into vector mesons*, *Phys. Rev. D* **45** (1992) 869 [INSPIRE].
- [9] A. Abada *et al.*, *Semi-leptonic decays of heavy flavours on a fine grained lattice*, *Nucl. Phys. B* **416** (1994) 675 [arXiv:hep-lat/9308007] [INSPIRE].
- [10] UKQCD Collaboration, *An ‘improved’ lattice study of semileptonic decays of D mesons*, *Phys. Rev. D* **51** (1995) 4905 [arXiv: hep-lat/9410012] [INSPIRE].

- [11] T. Bhattacharya and R. Gupta, *Semileptonic form-factors from lattice QCD*, [[arXiv:hep-ph/9409284](#)] [[INSPIRE](#)].
- [12] APE Collaboration, *Lattice calculation of D and B meson semileptonic decays using the Clover action at beta = 6.0 on APE*, *Phys. Lett. B* **345** (1995) 513 [[arXiv:hep-lat/9411011](#)] [[INSPIRE](#)].
- [13] M. Wirbel, B. Stech and M. Bauer, *Exclusive Semileptonic Decays of Heavy Mesons*, *Z. Phys. C* **29** (1985) 637 [[INSPIRE](#)]; G. Kramer and B. Lampe, *Two Jet Cross-Section in e^+e^- Annihilation*, *Z. Phys. C* **34** (1987) 497 [[INSPIRE](#)].
- [14] N. Isgur, D. Scora, B. Grinstein and M. B. Wise, *Semileptonic B and D Decays in the Quark Model*, *Phys. Rev. D* **39** (1989) 799 [[INSPIRE](#)]; D. Scora and N. Isgur, *Polarization in $\bar{B} \rightarrow D^*e^- \nu_e$ and $D \rightarrow \bar{K}^*e^+ \nu_e$* , *Phys. Rev. D* **40** (1989) 1491 [[INSPIRE](#)].
- [15] F. J. Gilman and R. L. Singleton, *Analysis of Semileptonic Decays of Mesons Containing Heavy Quarks*, *Phys. Rev. D* **41** (1990) 142 [[INSPIRE](#)].
- [16] P. Ball, V. M. Braun, H. G. Dosch, and M. Neubert, *Sum rule analysis of the decay $D^+ \rightarrow \bar{K}^{*0}e^+ \nu_e$* , *Phys. Lett. B* **259** (1991) 481 [[INSPIRE](#)]; P. Ball, V. M. Braun, and H. G. Dosch, *Form-factors of semileptonic D decays from QCD sum rules*, *Phys. Rev. D* **44**, (1991) 3567 [[INSPIRE](#)].
- [17] MARK-III Collaboration, *Measurement of the hadronic structure of semileptonic D^0 and D^+ decays*, *Phys. Rev. Lett.* **66** (1991) 1011 [[INSPIRE](#)].
- [18] CLEO Collaboration, *Analysis of $D^+ \rightarrow K^- \pi^+ e^+ \nu_e$ and $D^+ \rightarrow K^- \pi^+ \mu \nu_\mu$ Semeleptonic Decays*, *Phys. Rev. D* **81** (2010) 112001 [[arXiv:hep-ex/1004.1954](#)] [[INSPIRE](#)].
- [19] BABAR Collaboration, *Analysis of $D^+ \rightarrow K^- \pi^+ e^+ \nu_e$ decay channel*, *Phys. Rev. D* **83** (2011) 072001 [[arXiv:hep-ex/1012.1810](#)] [[INSPIRE](#)].
- [20] BESIII Collaboration, *Study of $D^+ \rightarrow K^- \pi^+ e^+ \nu_e$* , *Phys. Rev. D* **94** (2016) 032001 [[arXiv:hep-ex/1512.08627](#)] [[INSPIRE](#)].
- [21] PARTICLE DATA GROUP, *Review of Particle Physics*, *Prog. Theor. Exp. Phys* **2022** (2022) 083C01.
- [22] M. Ablikim *et al.* (BESIII Collaboration), BESIII Collaboration, *Measurement of the integrated luminosities of the data taken by BESIII at $\sqrt{s} = 3.650$ and 3.773 GeV*, *Chin. Phys. C* **37**, 123001 (2013) [[arXiv:hep-ex/1307.2022](#)] [[INSPIRE](#)]; *Measurement of the $e^+e^- \rightarrow \pi^+\pi^-$ cross section between 600 and 900 MeV using initial state radiation*, *Phys. Lett. B* **753**, 629-638 (2016) [[arXiv:hep-ex/1507.08188](#)] [[INSPIRE](#)]. These articles described the integrated luminosity measurement for data taken in 2010 and 2011. The integrated luminosity for data taken in 2022 is determined via a similar procedure.
- [23] BESIII Collaboration, *Design and Construction of the BESIII Detector*, *Nucl. Instrum. Meth. A* **614** (2010) 345 [[arXiv:physics.ins-det/0911.4960](#)] [[INSPIRE](#)].
- [24] C. H. Yu *et al.*, *BEPCII Performance and Beam Dynamics Studies on Luminosity*, *Proceedings of IPAC2016, Busan, Korea, 2016*. [[INSPIRE](#)].
- [25] BESIII Collaboration, *Future Physics Programme of BESIII*, *Chin. Phys. C* **44** (2020) 040001 [[arXiv:hep-ex/1912.05983](#)] [[INSPIRE](#)].
- [26] J. Lu, Y. Xiao, X. Ji, *Online monitoring of the center-of-mass energy from real data at BESIII*, *Radiat. Detect. Technol. Methods* **4** (2020) 337.

- [27] J. W. Zhang, L. H. Wu, S. S. Sun *et al.*, *Suppression of top-up injection backgrounds with offline event filter in the BESIII experiment*, *Radiat. Detect. Technol. Methods* **6** (2022) 289 [INSPIRE].
- [28] K. X. Huang, *et al.*, *Method for detector description transformation to Unity and application in BESIII*, *Nucl. Sci. Tech* **33** (2022) 142 [arXiv:physics.ins-det/2206.10117] [INSPIRE].
- [29] X. Li *et al.*, *Study of MRPC technology for BESIII endcap-TOF upgrade*, *Radiat. Detect. Technol. Methods* **1** (2017) 13; Y. X. Guo *et al.*, *The study of time calibration for upgraded end cap TOF of BESIII*, *Radiat. Detect. Technol. Methods* **1** (2017) 15 [INSPIRE]; P. Cao *et al.*, *Design and construction of the new BESIII endcap Time-of-Flight system with MRPC Technology*, *Nucl. Instrum. Meth. A* **953** (2020) 163053 [INSPIRE].
- [30] GEANT4 Collaboration, *GEANT4—a simulation toolkit*, *Nucl. Instrum. Meth. A* **506** (2003) 250 [INSPIRE].
- [31] S. Jadach, B. F. L. Ward, and Z. Was, *The Precision Monte Carlo event generator KK for two fermion final states in e^+e^- collisions*, *Comp. Phys. Commu* **130**, (2000) 260 [arXiv:hep-ph/9912214] [INSPIRE]; *Coherent exclusive exponentiation for precision Monte Carlo calculations*, *Phys. Rev. D* **63** (2001) 113009 [arXiv:hep-ph/0006359] [INSPIRE].
- [32] D. J. Lange, *The Precision Monte Carlo event generator KK for two fermion final states in e^+e^- collisions*, *Nucl. Instrum. Meth. A* **462** (2001) 152 [arXiv:hep-ph/9912214] [INSPIRE]; R. G. Ping, *Event generators at BESIII*, *Chin. Phys. C* **32** (2008) 599.
- [33] J. C. Chen, G. S. Huang, X. R. Qi, D. H. Zhang, and Y. S. Zhu, *Event generator for J/ψ and $\psi(2S)$ decay*, *Phys. Rev. D* **62** (2000) 034003.
- [34] E. Richter-Was, *QED bremsstrahlung in semileptonic B and leptonic tau decays*, *Phys. Lett. B* **303** (1993) 163 [INSPIRE].
- [35] MARK-III Collaboration, *Direct Measurements of Charmed d Meson Hadronic Branching Fractions*, *Phys. Rev. Lett.* **56** (1986) 2140 [INSPIRE]; MARK-III Collaboration, *A Reanalysis of Charmed d Meson Branching Fractions*, *Phys. Rev. Lett.* **60** (1988) 89 [INSPIRE].
- [36] ARGUS Collaboration, *Search for Hadronic $b \rightarrow \mu$ Decays*, *Phys. Lett. B* **241** (1990) 278 [INSPIRE].
- [37] BESIII Collaboration, *Search for the rare decays $J/\psi \rightarrow D^0 e^+ e^-$ and $\psi(3686) \rightarrow D^0 e^+ e^- + c.c.$* , *Phys. Rev. D* **96**, (2017) 111101 [arXiv:hep-ex/1710.02278] [INSPIRE].
- [38] BESIII Collaboration, *Measurement of the Branching Fraction For the Semi-Leptonic Decays $D^{0(+)} \rightarrow \pi^{-(0)} \mu^+ \nu_\mu$ and Test of Lepton Flavor Universality*, *Phys. Rev. Lett.* **121**, (2018) 171803 [arXiv:hep-ex/1802.05492] [INSPIRE].
- [39] BESIII Collaboration, *Observation for $D^0 \rightarrow K_1(1270)^- e^+ \nu_e$* , *Phys. Rev. Lett.* **127** (2021) 131801 [arXiv:hep-ex/2102.10850] [INSPIRE].
- [40] N. Cabibbo and A. Maksymowicz, *Angular Correlations in Ke-4 Decays and Determination of Low-Energy pi-pi Phase Shifts*, *Phys. Rev.* **137** (1965) B438 [INSPIRE].
- [41] A. Pais and S. B Treiman, *Pion Phase-Shift Information from K_{l4} Decays*, *Phys. Rev.* **168** (1968) 1858 [INSPIRE].
- [42] C. L. Y. Lee, M. Lu, and M.B. Wise, *B_{l4} and D_{l4} decay*, *Phys. Rev. D* **46** (1992) 5040 [INSPIRE].

- [43] J. M. Blatt and V. F. Weisskopf, *Theoretical Nuclear Physics*, New York: John Wiley & Sons (1952); S. U. Chung *et al.*, *Partial wave analysis in K matrix formalism*, *Ann. Phys.* **4**(1995) 404 [[INSPIRE](#)].
- [44] D. Aston *et al.*, *A Study of $K^- \pi^+$ Scattering in the Reaction $K^- p \rightarrow K^- \pi^+ n$ at 11-GeV/c*, *Nucl. Phys. B* **296** (1988) 493 [[INSPIRE](#)].
- [45] J. G. Korner and G. A. Schuler, *Exclusive Semileptonic Heavy Meson Decays Including Lepton Mass Effects*, *Z. Phys. C* **46**(1990) 93 [[INSPIRE](#)].
- [46] F. J. Gilman and R. L. Singleton, *Analysis of Semileptonic Decays of Mesons Containing Heavy Quarks*, *Phys. Lett.* **41**(1990) 142 [[INSPIRE](#)].
- [47] FOCUS Collaboration, *New Measurements of the $D^+ \rightarrow \bar{K}^{*0} \mu^+ \nu$ Form-Factor Ratios*, *Phys. Lett. B* **544**(2002) 89 [[arXiv:hep-ex/0207049](#)] [[INSPIRE](#)].
- [48] W. Verkerke and D.P. Kirkby, *RooFit Users Manual v2.91*.
- [49] F. James, *Monte Carlo Phase Space*, *CERN Report* (1968) 68-15.

M. Ablikim¹, M. N. Achasov^{4,c}, P. Adlarson⁷⁶, O. Afedulidis³, X. C. Ai⁸¹, R. Aliberti³⁵,
A. Amoroso^{75A,75C}, Q. An^{72,58,a}, Y. Bai⁵⁷, O. Bakina³⁶, I. Balossino^{29A}, Y. Ban^{46,h}, H.-R. Bao⁶⁴,
V. Batozskaya^{1,44}, K. Begzsuren³², N. Berger³⁵, M. Berlowski⁴⁴, M. Bertani^{28A}, D. Bettoni^{29A},
F. Bianchi^{75A,75C}, E. Bianco^{75A,75C}, A. Bortone^{75A,75C}, I. Boyko³⁶, R. A. Briere⁵,
A. Brueggemann⁶⁹, H. Cai⁷⁷, X. Cai^{1,58}, A. Calcaterra^{28A}, G. F. Cao^{1,64}, N. Cao^{1,64},
S. A. Cetin^{62A}, X. Y. Chai^{46,h}, J. F. Chang^{1,58}, G. R. Che⁴³, G. Chelkov^{36,b}, C. Chen⁴³,
C. H. Chen⁹, Chao Chen⁵⁵, G. Chen¹, H. S. Chen^{1,64}, H. Y. Chen²⁰, M. L. Chen^{1,58,64},
S. J. Chen⁴², S. L. Chen⁴⁵, S. M. Chen⁶¹, T. Chen^{1,64}, X. R. Chen^{31,64}, X. T. Chen^{1,64},
Y. B. Chen^{1,58}, Y. Q. Chen³⁴, Z. J. Chen^{25,i}, Z. Y. Chen^{1,64}, S. K. Choi¹⁰, G. Cibinetto^{29A},
F. Cossio^{75C}, J. J. Cui⁵⁰, H. L. Dai^{1,58}, J. P. Dai⁷⁹, A. Dbeyssi¹⁸, R. E. de Boer³, D. Dedovich³⁶,
C. Q. Deng⁷³, Z. Y. Deng¹, A. Denig³⁵, I. Denysenko³⁶, M. Destefanis^{75A,75C}, F. De Mori^{75A,75C},
B. Ding^{67,1}, X. X. Ding^{46,h}, Y. Ding³⁴, Y. Ding⁴⁰, J. Dong^{1,58}, L. Y. Dong^{1,64}, M. Y. Dong^{1,58,64},
X. Dong⁷⁷, M. C. Du¹, S. X. Du⁸¹, Y. Y. Duan⁵⁵, Z. H. Duan⁴², P. Egorov^{36,b}, Y. H. Fan⁴⁵,
J. Fang⁵⁹, J. Fang^{1,58}, S. S. Fang^{1,64}, W. X. Fang¹, Y. Fang¹, Y. Q. Fang^{1,58}, R. Farinelli^{29A},
L. Fava^{75B,75C}, F. Feldbauer³, G. Felici^{28A}, C. Q. Feng^{72,58}, J. H. Feng⁵⁹, Y. T. Feng^{72,58},
M. Fritsch³, C. D. Fu¹, J. L. Fu⁶⁴, Y. W. Fu^{1,64}, H. Gao⁶⁴, X. B. Gao⁴¹, Y. N. Gao^{46,h},
Yang Gao^{72,58}, S. Garbolino^{75C}, I. Garzia^{29A,29B}, L. Ge⁸¹, P. T. Ge¹⁹, Z. W. Ge⁴², C. Geng⁵⁹,
E. M. Gersabeck⁶⁸, A. Gilman⁷⁰, K. Goetzen¹³, L. Gong⁴⁰, W. X. Gong^{1,58}, W. Gradl³⁵,
S. Gramigna^{29A,29B}, M. Greco^{75A,75C}, M. H. Gu^{1,58}, Y. T. Gu¹⁵, C. Y. Guan^{1,64}, A. Q. Guo^{31,64},
L. B. Guo⁴¹, M. J. Guo⁵⁰, R. P. Guo⁴⁹, Y. P. Guo^{12,g}, A. Guskov^{36,b}, J. Gutierrez²⁷, K. L. Han⁶⁴,
T. T. Han¹, F. Hanisch³, X. Q. Hao¹⁹, F. A. Harris⁶⁶, K. K. He⁵⁵, K. L. He^{1,64}, F. H. Heinsius³,
C. H. Heinz³⁵, Y. K. Heng^{1,58,64}, C. Herold⁶⁰, T. Holtmann³, P. C. Hong³⁴, G. Y. Hou^{1,64},
X. T. Hou^{1,64}, Y. R. Hou⁶⁴, Z. L. Hou¹, B. Y. Hu⁵⁹, H. M. Hu^{1,64}, J. F. Hu^{56,j}, S. L. Hu^{12,g},
T. Hu^{1,58,64}, Y. Hu¹, G. S. Huang^{72,58}, K. X. Huang⁵⁹, L. Q. Huang^{31,64}, X. T. Huang⁵⁰,
Y. P. Huang¹, Y. S. Huang⁵⁹, T. Hussain⁷⁴, F. Hölzken³, N. Hüsken³⁵, N. in der Wiesche⁶⁹,
J. Jackson²⁷, S. Janchiv³², J. H. Jeong¹⁰, Q. Ji¹, Q. P. Ji¹⁹, W. Ji^{1,64}, X. B. Ji^{1,64}, X. L. Ji^{1,58},
Y. Y. Ji⁵⁰, X. Q. Jia⁵⁰, Z. K. Jia^{72,58}, D. Jiang^{1,64}, H. B. Jiang⁷⁷, P. C. Jiang^{46,h}, S. S. Jiang³⁹,
T. J. Jiang¹⁶, X. S. Jiang^{1,58,64}, Y. Jiang⁶⁴, J. B. Jiao⁵⁰, J. K. Jiao³⁴, Z. Jiao²³, S. Jin⁴², Y. Jin⁶⁷,
M. Q. Jing^{1,64}, X. M. Jing⁶⁴, T. Johansson⁷⁶, S. Kabana³³, N. Kalantar-Nayestanaki⁶⁵,
X. L. Kang⁹, X. S. Kang⁴⁰, M. Kavatsyuk⁶⁵, B. C. Ke⁸¹, V. Khachatryan²⁷, A. Khoukaz⁶⁹,
R. Kiuchi¹, O. B. Kolcu^{62A}, B. Kopf³, M. Kuessner³, X. Kui^{1,64}, N. Kumar²⁶, A. Kupsc^{44,76},
W. Kühn³⁷, J. J. Lane⁶⁸, L. Lavezzi^{75A,75C}, T. T. Lei^{72,58}, Z. H. Lei^{72,58}, M. Lellmann³⁵,
T. Lenz³⁵, C. Li⁴⁷, C. Li⁴³, C. H. Li³⁹, Cheng Li^{72,58}, D. M. Li⁸¹, F. Li^{1,58}, G. Li¹, H. B. Li^{1,64},
H. J. Li¹⁹, H. N. Li^{56,j}, Hui Li⁴³, J. R. Li⁶¹, J. S. Li⁵⁹, K. Li¹, K. L. Li¹⁹, L. J. Li^{1,64}, L. K. Li¹,
Lei Li⁴⁸, M. H. Li⁴³, P. R. Li^{38,k,l}, Q. M. Li^{1,64}, Q. X. Li⁵⁰, R. Li^{17,31}, S. X. Li¹², T. Li⁵⁰,
W. D. Li^{1,64}, W. G. Li^{1,a}, X. Li^{1,64}, X. H. Li^{72,58}, X. L. Li⁵⁰, X. Y. Li^{1,64}, X. Z. Li⁵⁹, Y. G. Li^{46,h},
Z. J. Li⁵⁹, Z. Y. Li⁷⁹, C. Liang⁴², H. Liang^{1,64}, H. Liang^{72,58}, Y. F. Liang⁵⁴, Y. T. Liang^{31,64},
G. R. Liao¹⁴, Y. P. Liao^{1,64}, J. Libby²⁶, A. Limphirat⁶⁰, C. C. Lin⁵⁵, D. X. Lin^{31,64}, T. Lin¹,
B. J. Liu¹, B. X. Liu⁷⁷, C. Liu³⁴, C. X. Liu¹, F. Liu¹, F. H. Liu⁵³, Feng Liu⁶, G. M. Liu^{56,j},
H. Liu^{38,k,l}, H. B. Liu¹⁵, H. H. Liu¹, H. M. Liu^{1,64}, Huihui Liu²¹, J. B. Liu^{72,58}, J. Y. Liu^{1,64},
K. Liu^{38,k,l}, K. Y. Liu⁴⁰, Ke Liu²², L. Liu^{72,58}, L. C. Liu⁴³, Lu Liu⁴³, M. H. Liu^{12,g}, P. L. Liu¹,
Q. Liu⁶⁴, S. B. Liu^{72,58}, T. Liu^{12,g}, W. K. Liu⁴³, W. M. Liu^{72,58}, X. Liu^{38,k,l}, X. Liu³⁹, Y. Liu⁸¹,
Y. Liu^{38,k,l}, Y. B. Liu⁴³, Z. A. Liu^{1,58,64}, Z. D. Liu⁹, Z. Q. Liu⁵⁰, X. C. Lou^{1,58,64}, F. X. Lu⁵⁹,
H. J. Lu²³, J. G. Lu^{1,58}, X. L. Lu¹, Y. Lu⁷, Y. P. Lu^{1,58}, Z. H. Lu^{1,64}, C. L. Luo⁴¹, J. R. Luo⁵⁹,
M. X. Luo⁸⁰, T. Luo^{12,g}, X. L. Luo^{1,58}, X. R. Lyu⁶⁴, Y. F. Lyu⁴³, F. C. Ma⁴⁰, H. Ma⁷⁹,
H. L. Ma¹, J. L. Ma^{1,64}, L. L. Ma⁵⁰, L. R. Ma⁶⁷, M. M. Ma^{1,64}, Q. M. Ma¹, R. Q. Ma^{1,64},
T. Ma^{72,58}, X. T. Ma^{1,64}, X. Y. Ma^{1,58}, Y. M. Ma³¹, F. E. Maas¹⁸, I. MacKay⁷⁰,
M. Maggiora^{75A,75C}, S. Malde⁷⁰, Y. J. Mao^{46,h}, Z. P. Mao¹, S. Marcello^{75A,75C}, Z. X. Meng⁶⁷,

J. G. Messchendorp^{13,65}, G. Mezzadri^{29A}, H. Miao^{1,64}, T. J. Min⁴², R. E. Mitchell²⁷,
 X. H. Mo^{1,58,64}, B. Moses²⁷, N. Yu. Muchnoi^{4,c}, J. Muskalla³⁵, Y. Nefedov³⁶, F. Nerling^{18,e},
 L. S. Nie²⁰, I. B. Nikolaev^{4,c}, Z. Ning^{1,58}, S. Nisar^{11,m}, Q. L. Niu^{38,k,l}, W. D. Niu⁵⁵, Y. Niu⁵⁰,
 S. L. Olsen⁶⁴, S. L. Olsen^{10,64}, Q. Ouyang^{1,58,64}, S. Pacetti^{28B,28C}, X. Pan⁵⁵, Y. Pan⁵⁷,
 A. Pathak³⁴, Y. P. Pei^{72,58}, M. Pelizaeus³, H. P. Peng^{72,58}, Y. Y. Peng^{38,k,l}, K. Peters^{13,e},
 J. L. Ping⁴¹, R. G. Ping^{1,64}, S. Plura³⁵, V. Prasad³³, F. Z. Qi¹, H. Qi^{72,58}, H. R. Qi⁶¹, M. Qi⁴²,
 T. Y. Qi^{12,g}, S. Qian^{1,58}, W. B. Qian⁶⁴, C. F. Qiao⁶⁴, X. K. Qiao⁸¹, J. J. Qin⁷³, L. Q. Qin¹⁴,
 L. Y. Qin^{72,58}, X. P. Qin^{12,g}, X. S. Qin⁵⁰, Z. H. Qin^{1,58}, J. F. Qiu¹, Z. H. Qu⁷³, C. F. Redmer³⁵,
 K. J. Ren³⁹, A. Rivetti^{75C}, M. Rolo^{75C}, G. Rong^{1,64}, Ch. Rosner¹⁸, S. N. Ruan⁴³, N. Salone⁴⁴,
 A. Sarantsev^{36,d}, Y. Schelhaas³⁵, K. Schoenning⁷⁶, M. Scodreggio^{29A}, K. Y. Shan^{12,g}, W. Shan²⁴,
 X. Y. Shan^{72,58}, Z. J. Shang^{38,k,l}, J. F. Shangguan¹⁶, L. G. Shao^{1,64}, M. Shao^{72,58}, C. P. Shen^{12,g},
 H. F. Shen^{1,8}, W. H. Shen⁶⁴, X. Y. Shen^{1,64}, B. A. Shi⁶⁴, H. Shi^{72,58}, H. C. Shi^{72,58}, J. L. Shi^{12,g},
 J. Y. Shi¹, Q. Q. Shi⁵⁵, S. Y. Shi⁷³, X. Shi^{1,58}, J. J. Song¹⁹, T. Z. Song⁵⁹, W. M. Song^{34,1}, Y.
 J. Song^{12,g}, Y. X. Song^{46,h,n}, S. Sosio^{75A,75C}, S. Spataro^{75A,75C}, F. Stieler³⁵, S. S. Su⁴⁰,
 Y. J. Su⁶⁴, G. B. Sun⁷⁷, G. X. Sun¹, H. Sun⁶⁴, H. K. Sun¹, J. F. Sun¹⁹, K. Sun⁶¹, L. Sun⁷⁷,
 S. S. Sun^{1,64}, T. Sun^{51,f}, W. Y. Sun³⁴, Y. Sun⁹, Y. J. Sun^{72,58}, Y. Z. Sun¹, Z. Q. Sun^{1,64},
 Z. T. Sun⁵⁰, C. J. Tang⁵⁴, G. Y. Tang¹, J. Tang⁵⁹, M. Tang^{72,58}, Y. A. Tang⁷⁷, L. Y. Tao⁷³,
 Q. T. Tao^{25,i}, M. Tat⁷⁰, J. X. Teng^{72,58}, V. Thoren⁷⁶, W. H. Tian⁵⁹, Y. Tian^{31,64}, Z. F. Tian⁷⁷,
 I. Uman^{62B}, Y. Wan⁵⁵, S. J. Wang⁵⁰, B. Wang¹, B. L. Wang⁶⁴, Bo Wang^{72,58}, D. Y. Wang^{46,h},
 F. Wang⁷³, H. J. Wang^{38,k,l}, J. J. Wang⁷⁷, J. P. Wang⁵⁰, K. Wang^{1,58}, L. L. Wang¹, M. Wang⁵⁰,
 N. Y. Wang⁶⁴, S. Wang^{38,k,l}, S. Wang^{12,g}, T. Wang^{12,g}, T. J. Wang⁴³, W. Wang⁷³, W. Wang⁵⁹,
 W. P. Wang^{35,58,72,o}, X. Wang^{46,h}, X. F. Wang^{38,k,l}, X. J. Wang³⁹, X. L. Wang^{12,g}, X. N. Wang¹,
 Y. Wang⁶¹, Y. D. Wang⁴⁵, Y. F. Wang^{1,58,64}, Y. L. Wang¹⁹, Y. N. Wang⁴⁵, Y. Q. Wang¹,
 Yaqian Wang¹⁷, Yi Wang⁶¹, Z. Wang^{1,58}, Z. L. Wang⁷³, Z. Y. Wang^{1,64}, Ziyi Wang⁶⁴,
 D. H. Wei¹⁴, F. Weidner⁶⁹, S. P. Wen¹, Y. R. Wen³⁹, U. Wiedner³, G. Wilkinson⁷⁰, M. Wolke⁷⁶,
 L. Wollenberg³, C. Wu³⁹, J. F. Wu^{1,8}, L. H. Wu¹, L. J. Wu^{1,64}, X. Wu^{12,g}, X. H. Wu³⁴,
 Y. Wu^{72,58}, Y. H. Wu⁵⁵, Y. J. Wu³¹, Z. Wu^{1,58}, L. Xia^{72,58}, X. M. Xian³⁹, B. H. Xiang^{1,64},
 T. Xiang^{46,h}, D. Xiao^{38,k,l}, G. Y. Xiao⁴², S. Y. Xiao¹, Y. L. Xiao^{12,g}, Z. J. Xiao⁴¹, C. Xie⁴²,
 X. H. Xie^{46,h}, Y. Xie⁵⁰, Y. G. Xie^{1,58}, Y. H. Xie⁶, Z. P. Xie^{72,58}, T. Y. Xing^{1,64}, C. F. Xu^{1,64},
 C. J. Xu⁵⁹, G. F. Xu¹, H. Y. Xu^{67,2,p}, M. Xu^{72,58}, Q. J. Xu¹⁶, Q. N. Xu³⁰, W. Xu¹, W. L. Xu⁶⁷,
 X. P. Xu⁵⁵, Y. Xu⁴⁰, Y. C. Xu⁷⁸, Z. S. Xu⁶⁴, F. Yan^{12,g}, L. Yan^{12,g}, W. B. Yan^{72,58}, W. C. Yan⁸¹,
 X. Q. Yan^{1,64}, H. J. Yang^{51,f}, H. L. Yang³⁴, H. X. Yang¹, T. Yang¹, Y. Yang^{12,g}, Y. F. Yang⁴³,
 Y. F. Yang^{1,64}, Y. X. Yang^{1,64}, Z. W. Yang^{38,k,l}, Z. P. Yao⁵⁰, M. Ye^{1,58}, M. H. Ye⁸, J. H. Yin¹,
 Junhao Yin⁴³, Z. Y. You⁵⁹, B. X. Yu^{1,58,64}, C. X. Yu⁴³, G. Yu^{1,64}, J. S. Yu^{25,i}, M. C. Yu⁴⁰,
 T. Yu⁷³, X. D. Yu^{46,h}, Y. C. Yu⁸¹, C. Z. Yuan^{1,64}, J. Yuan³⁴, J. Yuan⁴⁵, L. Yuan², S. C. Yuan^{1,64},
 Y. Yuan^{1,64}, Z. Y. Yuan⁵⁹, C. X. Yue³⁹, A. A. Zafar⁷⁴, F. R. Zeng⁵⁰, S. H. Zeng^{63A,63B,63C,63D},
 X. Zeng^{12,g}, Y. Zeng^{25,i}, Y. J. Zeng^{1,64}, Y. J. Zeng⁵⁹, X. Y. Zhai³⁴, Y. C. Zhai⁵⁰, Y. H. Zhan⁵⁹,
 A. Q. Zhang^{1,64}, B. L. Zhang^{1,64}, B. X. Zhang¹, D. H. Zhang⁴³, G. Y. Zhang¹⁹, H. Zhang⁸¹,
 H. Zhang^{72,58}, H. C. Zhang^{1,58,64}, H. H. Zhang³⁴, H. H. Zhang⁵⁹, H. Q. Zhang^{1,58,64},
 H. R. Zhang^{72,58}, H. Y. Zhang^{1,58}, J. Zhang⁸¹, J. Zhang⁵⁹, J. J. Zhang⁵², J. L. Zhang²⁰,
 J. Q. Zhang⁴¹, J. S. Zhang^{12,g}, J. W. Zhang^{1,58,64}, J. X. Zhang^{38,k,l}, J. Y. Zhang¹,
 J. Z. Zhang^{1,64}, Jianyu Zhang⁶⁴, L. M. Zhang⁶¹, Lei Zhang⁴², P. Zhang^{1,64}, Q. Y. Zhang³⁴,
 R. Y. Zhang^{38,k,l}, S. H. Zhang^{1,64}, Shulei Zhang^{25,i,q}, X. M. Zhang¹, X. Y. Zhang⁴⁰,
 X. Y. Zhang⁵⁰, Y. Zhang⁷³, Y. Zhang¹, Y. T. Zhang⁸¹, Y. H. Zhang^{1,58}, Y. M. Zhang³⁹,
 Yan Zhang^{72,58}, Z. D. Zhang¹, Z. H. Zhang¹, Z. L. Zhang³⁴, Z. Y. Zhang⁴³, Z. Y. Zhang⁷⁷, Z. Z.
 Zhang⁴⁵, G. Zhao¹, J. Y. Zhao^{1,64}, J. Z. Zhao^{1,58}, L. Zhao¹, Lei Zhao^{72,58}, M. G. Zhao⁴³,
 N. Zhao⁷⁹, R. P. Zhao⁶⁴, S. J. Zhao⁸¹, Y. B. Zhao^{1,58}, Y. X. Zhao^{31,64}, Z. G. Zhao^{72,58},
 A. Zhemchugov^{36,b}, B. Zheng⁷³, B. M. Zheng³⁴, J. P. Zheng^{1,58}, W. J. Zheng^{1,64}, Y. H. Zheng⁶⁴,

B. Zhong⁴¹, X. Zhong⁵⁹, H. Zhou⁵⁰, J. Y. Zhou³⁴, L. P. Zhou^{1,64}, S. Zhou⁶, X. Zhou⁷⁷,
X. K. Zhou⁶, X. R. Zhou^{72,58}, X. Y. Zhou³⁹, Y. Z. Zhou^{12,g}, Z. C. Zhou²⁰, A. N. Zhu⁶⁴, J. Zhu⁴³,
K. Zhu¹, K. J. Zhu^{1,58,64}, K. S. Zhu^{12,g}, L. Zhu³⁴, L. X. Zhu⁶⁴, S. H. Zhu⁷¹, T. J. Zhu^{12,g},
W. D. Zhu⁴¹, Y. C. Zhu^{72,58}, Z. A. Zhu^{1,64}, J. H. Zou¹, J. Zu^{72,58}

(BESIII Collaboration)

- ¹ *Institute of High Energy Physics, Beijing 100049, People's Republic of China*
² *Beihang University, Beijing 100191, People's Republic of China*
³ *Bochum Ruhr-University, D-44780 Bochum, Germany*
⁴ *Budker Institute of Nuclear Physics SB RAS (BINP), Novosibirsk 630090, Russia*
⁵ *Carnegie Mellon University, Pittsburgh, Pennsylvania 15213, USA*
⁶ *Central China Normal University, Wuhan 430079, People's Republic of China*
⁷ *Central South University, Changsha 410083, People's Republic of China*
⁸ *China Center of Advanced Science and Technology, Beijing 100190, People's Republic of China*
⁹ *China University of Geosciences, Wuhan 430074, People's Republic of China*
¹⁰ *Chung-Ang University, Seoul, 06974, Republic of Korea*
¹¹ *COMSATS University Islamabad, Lahore Campus, Defence Road, Off Raiwind Road, 54000
Lahore, Pakistan*
¹² *Fudan University, Shanghai 200433, People's Republic of China*
¹³ *GSI Helmholtzcentre for Heavy Ion Research GmbH, D-64291 Darmstadt, Germany*
¹⁴ *Guangxi Normal University, Guilin 541004, People's Republic of China*
¹⁵ *Guangxi University, Nanning 530004, People's Republic of China*
¹⁶ *Hangzhou Normal University, Hangzhou 310036, People's Republic of China*
¹⁷ *Hebei University, Baoding 071002, People's Republic of China*
¹⁸ *Helmholtz Institute Mainz, Staudinger Weg 18, D-55099 Mainz, Germany*
¹⁹ *Henan Normal University, Xinxiang 453007, People's Republic of China*
²⁰ *Henan University, Kaifeng 475004, People's Republic of China*
²¹ *Henan University of Science and Technology, Luoyang 471003, People's Republic of China*
²² *Henan University of Technology, Zhengzhou 450001, People's Republic of China*
²³ *Huangshan College, Huangshan 245000, People's Republic of China*
²⁴ *Hunan Normal University, Changsha 410081, People's Republic of China*
²⁵ *Hunan University, Changsha 410082, People's Republic of China*
²⁶ *Indian Institute of Technology Madras, Chennai 600036, India*
²⁷ *Indiana University, Bloomington, Indiana 47405, USA*
²⁸ *INFN Laboratori Nazionali di Frascati , (A)INFN Laboratori Nazionali di Frascati, I-00044,
Frascati, Italy; (B)INFN Sezione di Perugia, I-06100, Perugia, Italy; (C)University of Perugia,
I-06100, Perugia, Italy*
²⁹ *INFN Sezione di Ferrara, (A)INFN Sezione di Ferrara, I-44122, Ferrara, Italy; (B)University
of Ferrara, I-44122, Ferrara, Italy*
³⁰ *Inner Mongolia University, Hohhot 010021, People's Republic of China*
³¹ *Institute of Modern Physics, Lanzhou 730000, People's Republic of China*
³² *Institute of Physics and Technology, Peace Avenue 54B, Ulaanbaatar 13330, Mongolia*
³³ *Instituto de Alta Investigación, Universidad de Tarapacá, Casilla 7D, Arica 1000000, Chile*
³⁴ *Jilin University, Changchun 130012, People's Republic of China*
³⁵ *Johannes Gutenberg University of Mainz, Johann-Joachim-Becher-Weg 45, D-55099 Mainz,
Germany*
³⁶ *Joint Institute for Nuclear Research, 141980 Dubna, Moscow region, Russia*
³⁷ *Justus-Liebig-Universität Giessen, II. Physikalisches Institut, Heinrich-Buff-Ring 16, D-35392*

Giessen, Germany

- ³⁸ Lanzhou University, Lanzhou 730000, People's Republic of China
- ³⁹ Liaoning Normal University, Dalian 116029, People's Republic of China
- ⁴⁰ Liaoning University, Shenyang 110036, People's Republic of China
- ⁴¹ Nanjing Normal University, Nanjing 210023, People's Republic of China
- ⁴² Nanjing University, Nanjing 210093, People's Republic of China
- ⁴³ Nankai University, Tianjin 300071, People's Republic of China
- ⁴⁴ National Centre for Nuclear Research, Warsaw 02-093, Poland
- ⁴⁵ North China Electric Power University, Beijing 102206, People's Republic of China
- ⁴⁶ Peking University, Beijing 100871, People's Republic of China
- ⁴⁷ Qufu Normal University, Qufu 273165, People's Republic of China
- ⁴⁸ Renmin University of China, Beijing 100872, People's Republic of China
- ⁴⁹ Shandong Normal University, Jinan 250014, People's Republic of China
- ⁵⁰ Shandong University, Jinan 250100, People's Republic of China
- ⁵¹ Shanghai Jiao Tong University, Shanghai 200240, People's Republic of China
- ⁵² Shanxi Normal University, Linfen 041004, People's Republic of China
- ⁵³ Shanxi University, Taiyuan 030006, People's Republic of China
- ⁵⁴ Sichuan University, Chengdu 610064, People's Republic of China
- ⁵⁵ Soochow University, Suzhou 215006, People's Republic of China
- ⁵⁶ South China Normal University, Guangzhou 510006, People's Republic of China
- ⁵⁷ Southeast University, Nanjing 211100, People's Republic of China
- ⁵⁸ State Key Laboratory of Particle Detection and Electronics, Beijing 100049, Hefei 230026, People's Republic of China
- ⁵⁹ Sun Yat-Sen University, Guangzhou 510275, People's Republic of China
- ⁶⁰ Suranaree University of Technology, University Avenue 111, Nakhon Ratchasima 30000, Thailand
- ⁶¹ Tsinghua University, Beijing 100084, People's Republic of China
- ⁶² Turkish Accelerator Center Particle Factory Group, (A)Istinye University, 34010, Istanbul, Turkey; (B)Near East University, Nicosia, North Cyprus, 99138, Mersin 10, Turkey
- ⁶³ University of Bristol, (A)H H Wills Physics Laboratory; (B)Tyndall Avenue; (C)Bristol; (D)BS8 1TL
- ⁶⁴ University of Chinese Academy of Sciences, Beijing 100049, People's Republic of China
- ⁶⁵ University of Groningen, NL-9747 AA Groningen, The Netherlands
- ⁶⁶ University of Hawaii, Honolulu, Hawaii 96822, USA
- ⁶⁷ University of Jinan, Jinan 250022, People's Republic of China
- ⁶⁸ University of Manchester, Oxford Road, Manchester, M13 9PL, United Kingdom
- ⁶⁹ University of Muenster, Wilhelm-Klemm-Strasse 9, 48149 Muenster, Germany
- ⁷⁰ University of Oxford, Keble Road, Oxford OX13RH, United Kingdom
- ⁷¹ University of Science and Technology Liaoning, Anshan 114051, People's Republic of China
- ⁷² University of Science and Technology of China, Hefei 230026, People's Republic of China
- ⁷³ University of South China, Hengyang 421001, People's Republic of China
- ⁷⁴ University of the Punjab, Lahore-54590, Pakistan
- ⁷⁵ University of Turin and INFN, (A)University of Turin, I-10125, Turin, Italy; (B)University of Eastern Piedmont, I-15121, Alessandria, Italy; (C)INFN, I-10125, Turin, Italy
- ⁷⁶ Uppsala University, Box 516, SE-75120 Uppsala, Sweden
- ⁷⁷ Wuhan University, Wuhan 430072, People's Republic of China
- ⁷⁸ Yantai University, Yantai 264005, People's Republic of China
- ⁷⁹ Yunnan University, Kunming 650500, People's Republic of China

⁸⁰ Zhejiang University, Hangzhou 310027, People's Republic of China

⁸¹ Zhengzhou University, Zhengzhou 450001, People's Republic of China

^a Deceased

^b Also at the Moscow Institute of Physics and Technology, Moscow 141700, Russia

^c Also at the Novosibirsk State University, Novosibirsk, 630090, Russia

^d Also at the NRC "Kurchatov Institute", PNPI, 188300, Gatchina, Russia

^e Also at Goethe University Frankfurt, 60323 Frankfurt am Main, Germany

^f Also at Key Laboratory for Particle Physics, Astrophysics and Cosmology, Ministry of Education; Shanghai Key Laboratory for Particle Physics and Cosmology; Institute of Nuclear and Particle Physics, Shanghai 200240, People's Republic of China

^g Also at Key Laboratory of Nuclear Physics and Ion-beam Application (MOE) and Institute of Modern Physics, Fudan University, Shanghai 200443, People's Republic of China

^h Also at State Key Laboratory of Nuclear Physics and Technology, Peking University, Beijing 100871, People's Republic of China

ⁱ Also at School of Physics and Electronics, Hunan University, Changsha 410082, China

^j Also at Guangdong Provincial Key Laboratory of Nuclear Science, Institute of Quantum Matter, South China Normal University, Guangzhou 510006, China

^k Also at MOE Frontiers Science Center for Rare Isotopes, Lanzhou University, Lanzhou 730000, People's Republic of China

^l Also at Lanzhou Center for Theoretical Physics, Lanzhou University, Lanzhou 730000, People's Republic of China

^m Also at the Department of Mathematical Sciences, IBA, Karachi 75270, Pakistan

ⁿ Also at Ecole Polytechnique Federale de Lausanne (EPFL), CH-1015 Lausanne, Switzerland

^o Also at Helmholtz Institute Mainz, Staudinger Weg 18, D-55099 Mainz, Germany

^p Also at School of Physics, Beihang University, Beijing 100191, China

^q Also at Greater Bay Area Institute for Innovation, Hunan University, Guangzhou 511300, China